THE ASTRONOMICAL JOURNAL, 121:2895–2914, 2001 June

CALTECH FAINT GALAXY REDSHIFT SURVEY. XIII. SPECTRAL ENERGY DISTRIBUTIONS FOR GALAXIES IN THE REGION OF THE HUBBLE DEEP FIELD NORTH[1]

JUDITH G. COHEN[2]
Received 2000 May 15; accepted 2001 March 12

ABSTRACT

We introduce a new empirical function for modeling the spectral energy distributions (SEDs) of galaxies. We apply it to a sample of 590 galaxies in the region of the Hubble Deep Field (HDF) with $z < 1.5$ using multicolor photometry with wide wavelength coverage combined with spectroscopic redshifts from our 93% complete *R*-selected redshift survey there. We find the following:

1. As expected, galaxies with strong signs of recent star formation (i.e., those that show emission lines) have bluer continua in both the rest-frame ultraviolet and optical/near-infrared.
2. The redder galaxies tend to be more luminous. Although galaxies with strong absorption lines and no emission features are $\sim 15\%$ of the total sample with $0.25 < z < 0.8$, they are $\sim 50\%$ of the 25 most luminous galaxies in the sample at rest-frame *R*.
3. The SEDs of actively star-forming galaxies become bluer in the mean in the rest-frame UV at higher redshifts, a trend that might arise from SED modeling errors. Aside from this, we discern no change with redshift in the relationship between SED characteristics and galaxy spectral type based on the strength of narrow emission and absorption features.
4. Combining with similar work at higher and lower redshift, the bluest galaxies have indistinguishable SEDs in the rest-frame UV over the redshift regime of 0–3.
5. There is no evidence in our *R*-selected sample that supports the existence of a substantial population of very dusty star-forming galaxies at $z \lesssim 1.5$.
6. Our ability to predict the mid-IR flux using the UV, optical, and near-IR SEDs is limited.
7. The potential accuracy of photometric redshifts is evaluated, bearing in mind that a break at 4000 Å must be detectable to within the errors of the photometry to assign a photo-*z* for galaxies in this redshift regime.
8. The rest-frame *K*-band luminosity as a function of redshift clearly shows a gradual change in the population of various types of galaxies, with star-forming galaxies becoming both more luminous and a larger fraction of the total population at higher redshifts.
9. The overall pattern of the $L(K)$-z relationship suggests that passive evolution at constant stellar mass is a good approximation to the actual behavior of at least the most luminous galaxies in this large sample of galaxies in the region of the HDF out to $z \sim 1.5$.

Key words: cosmology: observations — galaxies: fundamental parameters — galaxies: luminosity function, mass function — surveys

On-line material: machine-readable table

1. INTRODUCTION

In the present paper, we combine the results of our redshift survey in the region of the Hubble Deep Field North (hereafter HDF-N; Cohen et al. 2000) with multicolor photometric databases to derive the rest-frame spectral energy distributions (hereafter SEDs) of the sample's galaxies. After defining the form of the SED we adopt and exploring the limits of the validity thereof, we concentrate on what can be determined from the behavior of the SED parameters themselves as a function of redshift, galaxy spectral type (i.e., the presence or absence of key emission and absorption features), and luminosity. A comparison of the observed behavior of the SED parameters with the predictions of galaxy evolutionary synthesis models reveals important differences.

The SEDs of the star-forming galaxies are then used to constrain the possible presence of a substantial population of dusty starburst galaxies and to test our ability to predict the mid-IR thermal emission from dust in star-forming galaxies in § 5.3. Constraints on the variation in internal reddening from galaxy to galaxy of a given spectral type are derived as well. We compare the rest-frame UV SEDs of the bluest star-forming galaxies over the regime $z = 0$ to ~ 3.

We also evaluate the ability of photometric redshift schemes to discern the 4000 Å break, given realistic SED distributions and errors characteristic of ground-based photometry in § 6. In § 7, we explore the conversion from luminosity in the rest-frame IR into total stellar mass, which relies on a calibration from models of the integrated light of evolving galaxies. A short summary concludes the paper.

As in earlier papers in this series, we adopt the cosmology $H_0 = 60$ km s^{-1} Mpc^{-1}, $\Omega_M = 0.3$, and $\Omega_\Lambda = 0$. Over the

[1] Based in large part on observations obtained at the W.M. Keck Observatory, which is operated jointly by the California Institute of Technology, the University of California, and the National Aeronautics and Space Administration.

[2] Palomar Observatory, Mail Stop 105-24, California Institute of Technology, Pasadena, CA 91125.

redshift interval of most interest, a flat universe with $\Omega_\Lambda = 0.7$ and a Hubble constant of $H_0 = 67$ km s^{-1} Mpc^{-1} gives galaxy luminosities very close to those derived below.

2. SAMPLE OF GALAXIES

We have recently completed an extensive redshift survey in the region of the HDF-N. The survey is magnitude-limited with a selection at R, and objects are observed irrespective of morphology. Redshifts have been obtained for more than 92% of the objects in the HDF-N (Williams et al. 1996) with $R < 24$ and for more than 92% of the objects within a circle whose diameter is 8′ centered on the HDF-N with $R < 23$. The redshift catalog, presented and described in detail in Cohen et al. (2000), contains 671 entries. Hogg et al. (2000; hereafter H00) present a four-filter photometric catalog for the region of the HDF-N, including the flanking fields, with images in U_n, G, and R contributed by C. Steidel, and it is their R catalog that was used to define the samples for the redshift survey.

Appendix A gives an update to this survey with a total of 58 new redshifts, including five in the HDF-N itself. With this addition, the completion of the redshift sample in the HDF-N itself to $R \leq 24$ is now 95%, while the completion in the flanking fields to $R < 23$ is now 93%.

Here we use only the sample of galaxies with $0 < z < 1.5$, eliminating the Galactic stars, the two broad-lined AGN with $z < 1.5$, and the higher redshift ($z \sim 3$) objects,[3] leaving 590 galaxies. We do this since our ground-based photometry is measuring largely the rest-frame UV for $z \sim 3$ galaxies and does not provide enough coverage in the infrared to yield an adequate determination of rest-frame optical SEDs.

The rest-frame UV is very poorly determined in the nearest galaxies with $z < 0.25$ when photometry is limited to ground-based photometry without access to space-based mid- and far-UV observations. Hence, they are eliminated in the rest of this paper. Although SEDs are determined and tabulated for galaxies with $z < 0.25$ here, we will use in the subsequent discussion the sample of galaxies restricted to the range $0.25 < z < 1.5$, which contains 552 galaxies, of which 107 are in the HDF-N itself.

The results presented throughout this paper are robust to the elimination of the fainter galaxies in the HDF-N, where the sample is deepest.

2.1. *Redshift Ranges*

The present sample of galaxies in the region of the HDF-N, with $0.25 < z < 1.5$ and SEDs considered to be reliable, contains 519 galaxies, of which 105 are in the HDF-N itself.[4] These are divided into four redshift ranges: "low" ($0.25 \leq z < 0.5$), "mid" ($0.5 \leq z < 0.8$), "high" ($0.8 \leq z < 1.05$), and "highest" ($1.05 \leq z \leq 1.5$). In the highest redshift range, the assignment of galaxy spectral classes is less accurate (see the discussion in Cohen et al. 1999a), and the redshift completeness is affected by the fact that the intrinsically strong [O II] 3727 Å emission line is shifted into the region beyond 7500 Å, where strong night-sky emission lines make detection of faint emission lines from distant galaxies more difficult.

[3] The two AGNs with $z < 1.5$ are sometimes included in the figures.

[4] In § 3.8, we find that 33 of the galaxies have SEDs not considered to be reliable.

3. DERIVATION OF THE SEDs

The derivation of the SED for a galaxy requires a set of photometric measurements for the object with N filters, a set of effective wavelengths and flux zero-point calibrations for the filters, and a model for fitting the SED. Our goal is an overall characterization of the SED suitable for the determination of luminosity functions, given the fact that we are dealing, to a large extent, with ground-based photometry of faint galaxies.

We are trying to obtain a set of redshift-independent parameters, characterizing the rest-frame SED of a galaxy from a set of observations made at filter bandpasses fixed in the observed frame. We would like to be able to use our SED model parameters to predict fluxes of galaxies from 2400 Å to 2.2 μ in the rest frame over the redshift range $0.25 \leq z \leq 1.5$ with an accuracy of 25% (0.1 dex).

The complexity of the SED model to be used here is restricted by the limited photometry available for these objects, both in terms of accuracy for these faint galaxies and wavelength sampling. Were we dealing with *Hubble Space Telescope* (*HST*) data only (for the same set of filters) or with much brighter galaxies, a much more sophisticated approach, such as that of Budavári et al. (2000), would be justified.

3.1. *Sources of Photometry*

Since the catalog of H00 was used to define the sample for the redshift survey of Cohen et al. (2000) and since it provides four-filter photometry (U_n, G, R, and K_s) for the entire sample, we adopt it as the primary photometric source. The H00 photometry is consistent to within the uncertainties with the more accurate photometry of Williams et al. (1996) for objects in the HDF-N itself for the optical colors. In the flanking fields around the HDF-N, we supplement the photometric database of H00 with the I and K measurements of Barger et al. (1999). We used primarily I from Barger et al. (1999) to fill in gaps in the wavelength coverage of H00. For the faintest objects (in the infrared) in the flanking fields, we used K as well, since the limiting magnitude of the Barger et al. (1999) database is fainter at K than that of H00. The U, B, V, and R bands of Barger et al. are used to supply added confidence in the U_n, G, and R photometry of H00. Thus, for an object in the flanking fields, there is a maximum of 10 observations, with two independent measurements for three colors (U, R, and K), hence seven distinct filter bandpasses.

Within the HDF-N, in addition to the photometric catalog of H00, we also use the I, J, H, and K photometry of Fernández-Soto, Lanzetta, & Yahil (1999). Their catalog is based on the *HST* images of the HDF-N with the F814W filter for I and on their analysis of IR images of the HDF-N from KPNO described in Dickinson (2000). The red end of the SED is thus better determined for galaxies in the HDF-N itself because of the existence of the J and H photometry and the very high quality of the F814W *HST* images compared with ground-based I images.

The H00 and Fernández-Soto et al. (1999) photometric databases appear to be consistent with each other. They both use the SExtractor code (Bertin & Arnouts 1996) for object selection, and both have a scheme to handle extended objects, yet still preserve accuracy for the smallest and faintest galaxies. The unpublished photometry of Barger et al. (1999) treats the extrapolation to the total magnitude of

extended objects differently from the procedure adopted in H00.

We have adopted a single effective wavelength for each filter for all objects, irrespective of their spectral indexes, ignoring any dependence of $\lambda_{\rm eff}$ on the color of the object. This is a reasonable assumption given the precision of our photometry for faint objects and the desired precision of the SED indexes to be derived. The effective wavelengths of the various filters are given in Appendix B.

Once the effective wavelengths were defined, the zero points of the observed flux, f_ν, for the Vega-relative photometry were taken from Fukugita, Shimasaku, & Ichikawa (1995). The HDF-N photometry of Fernández-Soto et al. (1999) is already presented in the form of observed flux per unit frequency f_ν.

A small extinction of $E(B-V) = 0.012$ mag was adopted based on the maps of Schlegel, Finkbeiner, & Davis (1998); appropriate corrections were applied to each filter.

Our photometric database covers U through K in the observed frame. The red end of this corresponds to 0.9 μ in the rest frame of the highest redshift considered here and to $\sim$1.3 μ for a more typical $z \sim 0.7$ galaxy. Prediction of fluxes in the rest frame redward of 0.9 μ requires trusting the parametric form of our adopted SED model described below for the highest redshift galaxies in the sample.

3.2. *Dual Power-Law Model for the SEDs*

We initially adopted the same form for SEDs as Cohen et al. (1999a), namely, we assume that the emitted luminosity per unit frequency in the rest frame over the wavelength regime 0.2–1.6 μ can be represented by a power law whose index may change at 4000 Å. Thus L_ν, with units of watts per hertz, is assumed to be $\sim \nu^{-\alpha}$, with an index in the region redward of 4000 Å (in the rest frame), denoted by $\alpha_{\rm IR}$, and an index in the rest-frame UV of $\alpha_{\rm UV}$. Three parameters are required to characterize each SED. We refer to this as the 2p SED model.

Several tests of the validity of this model have been made to establish the wavelength range over which it can represent galaxy SEDs with the requisite degree of precision. Both SEDs from calculations of the integrated light of evolving galaxies and SEDs interpolated from spectrophotometric and broadband photometric observations of nearby galaxies have been used in these trials. In the first test, we fit the galaxy evolution models of Poggianti (1997), using the filter transmission curves for the set of filters for which photometric catalogs exist in the region of the HDF-N. Figure 1*a* illustrates SEDs from Poggianti (1997) of a local elliptical, Sa, and Sc galaxy (denoted as the standard set of test SEDs) observed at $z = 0.6$. The observed filter bands are the large filled circles plotted at their appropriate rest wavelengths. While the spectral region beyond the 4000 Å break for all the models from Poggianti (1997) that were examined is well represented by a single power law with deviations never exceeding 0.1 dex, the 2p model systematically predicts too much flux beyond 1.7 μ.

Tests of the 2p model were also carried out with galaxy SEDs predicted from Worthey (1994) and a set of SEDs of nearby galaxies of various morphological types constructed by G. Neugebauer (2000, private communication), based on

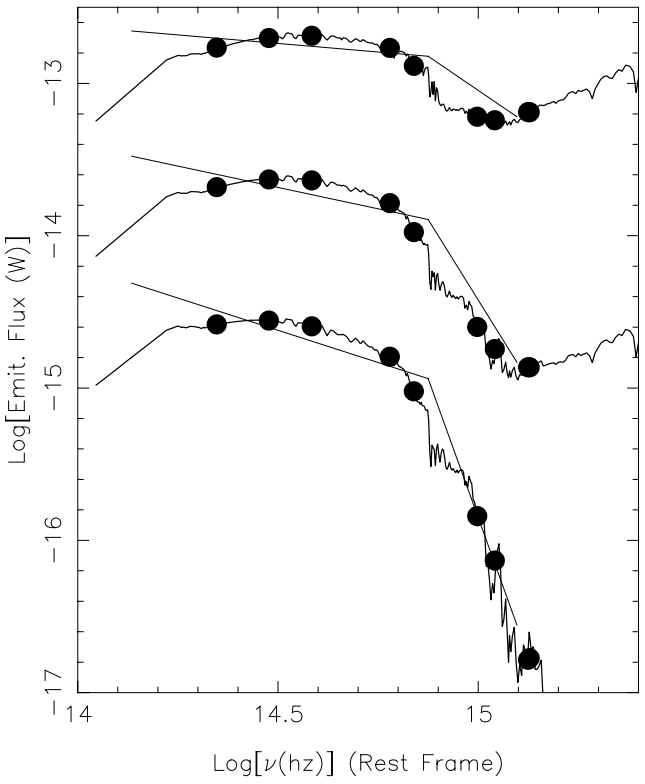

Fig. 1*a*

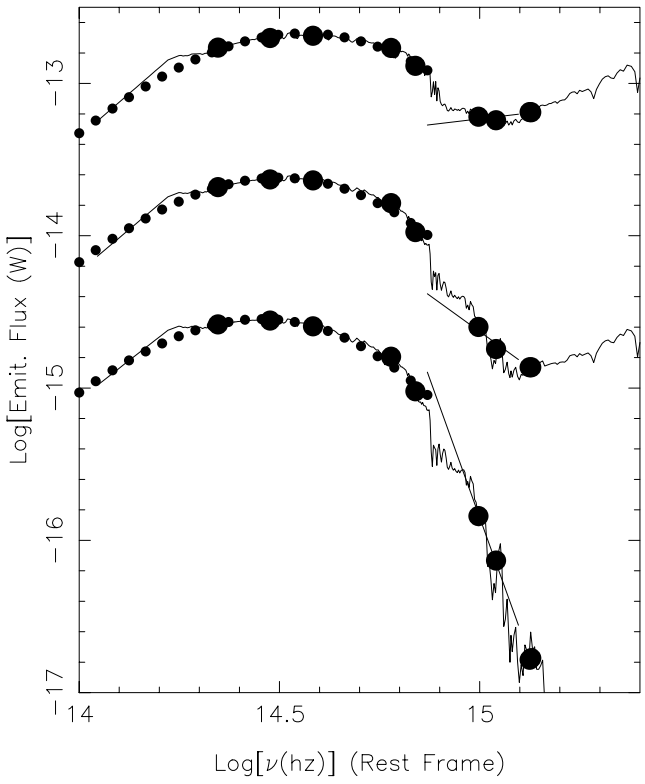

Fig. 1*b*

FIG. 1.—(*a*) The SEDs of $z = 0$ elliptical, Sa, and Sc galaxies from Poggianti (1997), shown as the curves, are observed at a redshift of 0.6. The resulting filter bands are indicated by the large filled circles. The 2p SED model is then fit to this set of filter data, and the UV and IR fit for each of the three SEDs is shown as a straight line. (*b*) Same as (*a*), but using the sBB SED model. The best fit is shown by small filled circles for the sBB function and a solid line for the power law in the UV.

observations in the UV and optical assembled by Coleman, Wu, & Weedman (1980), and supplemented with broadband IR photometry from Aaronson (1978) and Frogel et al. (1978). In all cases, the 2p SED overpredicts the flux in the near-IR.

We compare the predicted flux at an observed wavelength of 3.2 μ from our SED model with those galaxies in the HDF-N with detections at that wavelength from Hogg et al. (2000a). Given the typical redshift of these galaxies of $z \sim 0.5$, these observations have a typical rest wavelength of 2.1 μ. Again, the 2p model for the SED overpredicts the observed flux for the nine galaxies with detections by about a factor of 2.

This deviation in the near-IR between the power law and the galaxy flux presumably largely arises because one is then well into the long-wavelength tail of a blackbody distribution, in which even for T as low as 4000 K, f_λ is no longer rising rapidly with λ.

In the UV, the high spectral resolution of the Poggianti model grid demonstrates the existence of a different possible concern. Many of Poggianti's models show f_λ falling shortward of the 4000 Å break and then rising again as flux from the youngest and hottest stars begins to contribute substantially. This curvature obviously cannot be reproduced well by a single power-law flux in the UV. These tests demonstrate that the 2p model SED is, at best, marginally adequate for our purposes.

3.3. *New Empirical Model for Galaxy SEDs*

To avoid the difficulties of the 2p SED model described above, we have developed a new model for galaxy SEDs. One natural way to introduce the desired curvature in the optical and near-IR spectra region is to replace the power law with a blackbody function. However, the peak of the Planck function itself is too narrow to give a good fit to actual galaxy SEDs, as one might expect for a composite stellar population containing stars with a range of effective temperatures. The empirically determined function we adopt as our SED model, which provides a simple but versatile parameterization of galaxy SEDs with parameters that are physically motivated, has a mathematical form that we denote as a "stretched blackbody" (henceforth sBB). We apply the sBB function to fit the optical/near-IR, while we retain a power-law fit to the UV.

A wavelength λ_m is specified as the wavelength at which the fit function changes. The "stretched wavelength," λ_s, corresponding to a rest-frame wavelength λ_0, is then defined as

$$\lambda_s = \lambda_m + (\lambda_0 - \lambda_m)/f$$

for $\lambda_0 \geq \lambda_m$, where f is the stretch factor. To evaluate the sBB Planck function, the stretched wavelength is converted to a frequency in the usual way, $\nu_s = c/\lambda_s$, and then used in the calculation. This applies to both the ν^3 and exponential part of the Planck function, as well as the ν multiplier required to obtain luminosities. The temperature used in the Planck function is denoted as T(sBB). The details of the fitting procedure are given in Appendix C.

It is important to note that in this model, unlike in the 2p SED model, the flux at λ_m from the red fit and the blue fit is not automatically constrained to be the same. This offers the possibility of direct measurement of the 4000 Å break, which in cool stars is due to enhanced absorption by metal lines and in hotter stars by the Balmer jump. An sBB fit thus has four parameters, α_{UV}, T(sBB), the blue-side luminosity, and the red-side luminosity, both at λ_m. As described in Appendix C, depending on the number and distribution with wavelength of the available filter bandpasses (i.e., photometric catalogs), the two luminosity parameters are not always independent.

There are two constants in a sBB fit, λ_m and the wavelength stretching factor f. Their values were determined by optimizing χ^2 when a sBB fit was applied to the standard test set of Poggianti's (1997) local galaxy SEDs observed at $z = 0$ and $z = 0.6$. The resulting choices adopted hereafter for sBB fits are $\lambda_m = 4050$ Å and $f = 1.6$.

Figure 1*b* shows the sBB fit to the set of standard test SEDS, i.e., the same SEDs as are shown in Figure 1*a*. The sBB fit solves the problem of overpredicting the rest-frame flux at K, and with only one extra parameter, the sBB model shows a much better fit overall to predicted galaxy SEDs, as well as allowing a measurement of the 4000 Å break.

3.4. *Stability of the SED Parameters with Redshift*

The model SED must measure the same values for its parameters, irrespective of the redshift of a galaxy. Otherwise, the flux cannot be predicted reliably at a fixed rest wavelength. This is particularly difficult at K, since we are then extrapolating beyond the rest-frame wavelength range of the available photometry for $z > 0$. As pointed out by the referee, the 2p SED model fails this test. Figure 2 shows the output parameters from this model, α_{UV} and α_{IR}, applied to the set of standard local test SEDs as the redshift of observation is varied from 0 to 1.5. (The dependence of α_{UV} in the region $z < 0.25$ should be ignored; see § 2.) Note the large changes in output parameters for the 2p model SED as the redshift at which the galaxy is observed is varied.

This translates into predictions of flux using the 2p SED model that are, at the extremes of the rest-wavelength range covered, so different from those of the actual SED that our accuracy tolerance is grossly exceeded. Figure 3 shows the deviation from the fluxes of the standard test set of local SEDs predicted by the 2p SED model as the observations are carried out over the redshift range of interest, from $z = 0$ to 1.5. Results at four rest wavelengths, the two wavelength extremes of our range, 2400 Å and 2.2 μ, and at two intermediate wavelengths, 4350 and 7900 Å, are illustrated. As expected, the ability of the 2p SED model to predict the flux at the extreme ends of the wavelength range is poor, although in the central part of the wavelength range, it is reasonably good.

Figures 4 and 5 show the equivalent tests applied to the sBB model. Note that Figures 3 and 5 are directly comparable; the same rest wavelengths, axis scales, and plot symbols are used in both cases. We see that the predictive ability of the sBB fit is quite good; over the full redshift range $0 < z < 1.5$, the rest-frame flux at K is predicted to within ± 0.1 dex (our required tolerance), while the rest-frame flux at 2400 Å is predicted almost as accurately for $0.25 < z < 1.5$.

At this point, with the sBB fits, the worst remaining problem is now in the rest-frame UV (see Fig. 4). The overall trend toward measuring a bluer α_{UV} as z increases, particularly for the Sa and Sc SEDs, is probably due to an attempt to fit a curved SED that is "convex upward" as the contribution from younger stars increases and changes the curvature. In spite of this, we note that the flux prediction of

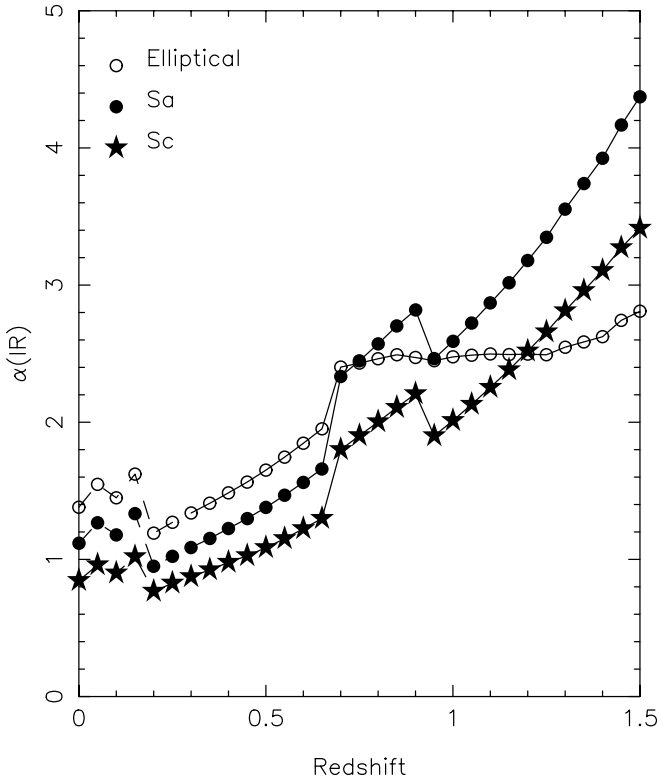

Fig. 2*a*

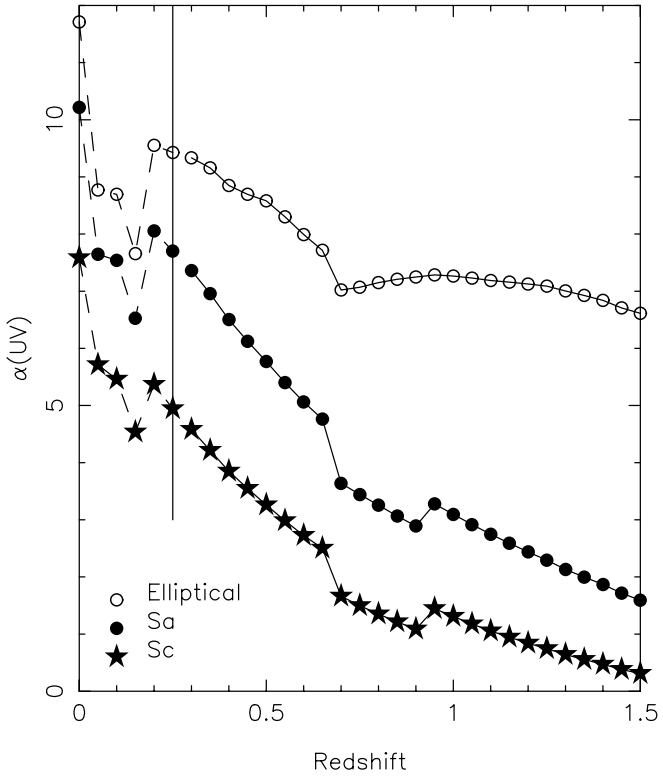

Fig. 2*b*

FIG. 2.—UV and IR power-law indices found from the 2p model of galaxy SEDs shown for the standard test set of local SEDs (those of Fig. 1). The redshift of observation ranged from $z = 0.0$ to 1.5. Open circles denote the track of the SED parameters determined for a local elliptical galaxy SED, filled circles show that of a local Sa, and stars show that of a local Sc galaxy. The vertical line in (*a*) reminds us that the UV fit is not considered valid in the region of $z < 0.25$.

the sBB model at 2400 Å shown in Figure 5 is still close to or within our tolerances.

These tests have been repeated for the sBB model, omitting the *J*- and *H*-band coverage, as occurs in the flanking fields of the HDF-N, in contrast with the HDF-N itself, where *J* and *H* photometry is available. The sBB fits are still very good and remain within the specified tolerance until $z > 1.1$.

3.5. *Final Comments on the SED Models*

Extrapolation beyond rest-frame *K* or blueward of 2400 Å of our adopted form for galaxy SEDs is not appropriate. Additional data on the 1.5–5 μ SEDs of nearby galaxies at better spectral resolution than is provided by standard broadband IR photometry would be helpful for improving the accuracy of galaxy synthesis models in the near-IR.

3.6. *Reddening*

We have tried adding additional reddening to the SEDs of local galaxies, both observed and synthesized from models. As one might expect, an additional reddening of $A_V = 1$ mag, with the standard Galactic extinction curve, produces an increase in $\alpha_{\rm UV}$ of ~ 2 and an increase in $\alpha_{\rm IR}$ of ~ 0.5. The fit over the wavelength range of interest is degraded, although not beyond the limit of acceptability, until the additional A_V reaches 2 mag. As we will see later, the range of the indexes $\alpha_{\rm UV}$ and $\alpha_{\rm IR}$ within each galaxy spectral type is sufficiently small that a range in reddening within each galaxy spectral type significantly exceeding $\sigma(A_V) = 1$ mag can be ruled out. However, a much larger range in reddening can be tolerated if it is grayer than the standard Galactic extinction curve, and has, for example, the form advocated by Calzetti (1997).

3.7. *Construction of the SEDs*

The SEDs for the galaxies in the region of the HDF-N were constructed by calculating, for each filter bandpass for which photometry exists, the quantity $\nu L_\nu = 4\pi D_L^2 \nu f_\nu = \nu_0 L_{\nu_0}$, where ν is the observed frequency, and ν_0 is the rest-frame frequency (D_L is the luminosity distance in our adopted cosmology). We then shift the observed effective wavelengths into the rest frame. For each galaxy, a plot was made of the raw SED that was then inspected manually. For about 10% of the objects, one deviant point, presumably corresponding to one bad measurement, was adjusted. In addition, the difference in large aperture extrapolation between the H00 and Barger et al. data sets had to be removed. Our magnitude zero point is based on that of H00.

A fit to the set of *N* values of νL_ν for each galaxy was then attempted. Details of fitting procedures and how the luminosity at the matching point is handled are given in Appendix C.

The resulting parameters for each galaxy for the 2p SEDs are the rest-frame emitted luminosity at *B*, $L(B) \equiv \nu L_\nu$, evaluated at *B* in the rest frame, and the two power-law indices. The range of $\pm 1\ \sigma$ values for $\alpha_{\rm UV}$ was from 0.2 to 0.9, with a typical value of ~ 0.5 in the flanking fields and ~ 0.4 in the HDF-N itself. For the sBB fits, the resulting parameters are $\alpha_{\rm UV}$, T, $L(\lambda_m$, blue), and $L(\lambda_m$, red). These values are given in Table 1 for our sample.

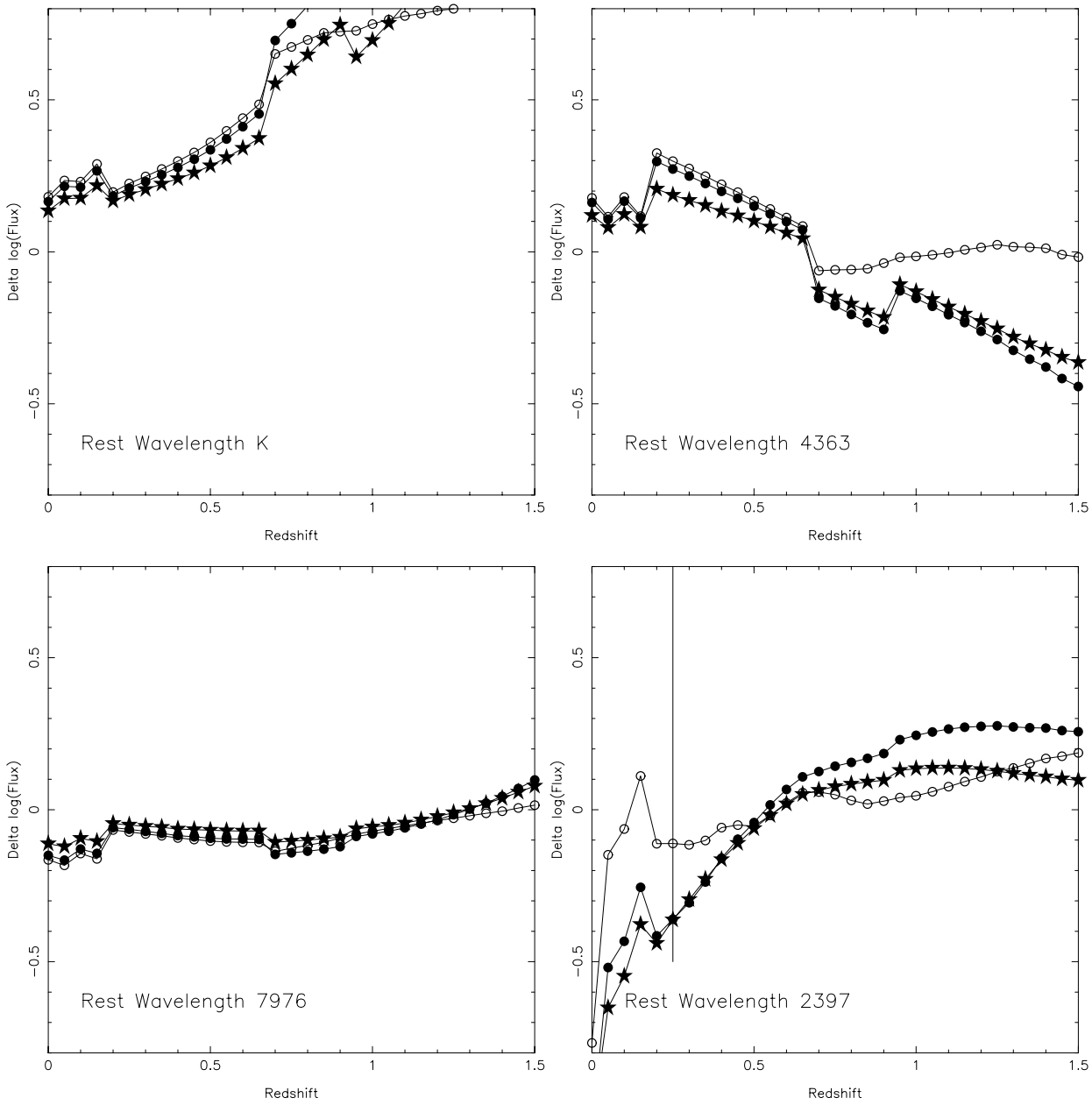

FIG. 3.—Rest-frame galaxy luminosity $L(\nu_0)$ predicted by the best-fit 2p SED model compared with the actual luminosity of the standard test set of local galaxy SEDs, which are observed over the range in redshift from 0 to 1.5. The plot symbols are the same as those of Fig. 2. The four panels give the results for four different rest wavelengths.

TABLE 1

SED PARAMETERS FOR OBJECTS IN THE REGION OF THE HDF-N

R.A. (J2000)	Decl. (J2000)	$\log L(B)$ (W)[a]	α_{UV} (2p)	α_{IR} (2p)	α_{UV} (sBB)	$\log L(\lambda_m$, blue) (W)	T (sBB)	$\log L(\lambda_m$, red) (W)
12 36 15.90	+62 12 37.3	36.90	2.61	0.65	1.32	36.69	5712	36.66
12 36 17.60	+62 14 02.2	36.93	0.91	0.68	0.71	36.92	7311	36.95
12 36 17.69	+62 13 44.3	36.84	6.01	1.65	7.12	36.77	4662	36.74
12 36 17.65	+62 14 08.1	36.71	1.40	1.53	1.07	36.64	5631	36.79
12 36 18.70	+62 11 54.1	36.63	2.43	1.73	2.54	36.62	5134	36.73

NOTES.—Units of right ascension are hours, minutes, and seconds, and units of declination are degrees, arcminutes, and arcseconds. Table 1 is presented in its entirety in the electronic edition of the Astronomical Journal. A portion is shown here for guidance regarding its form and content.

[a] $M_B = -21.0$ (rest frame) $\equiv \log [L(B)\ (\mathrm{W})] = 36.9$.

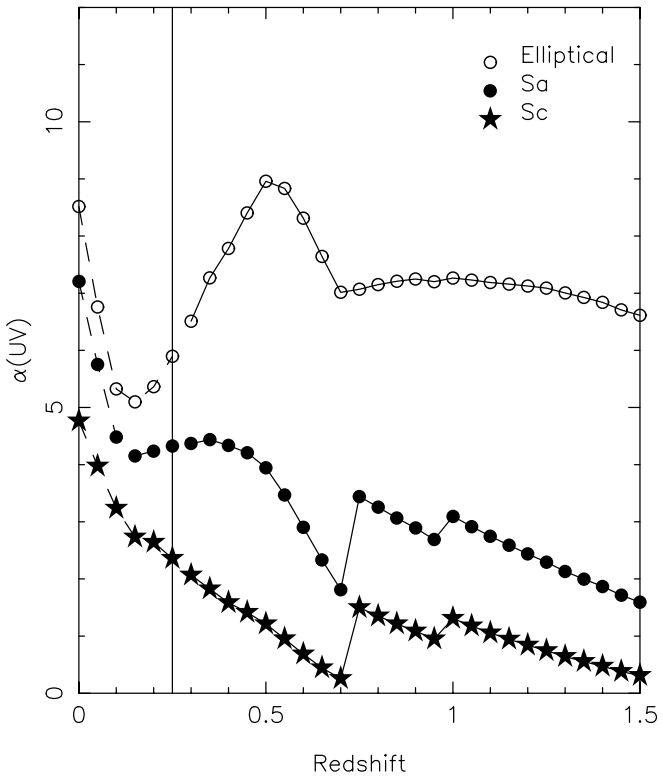

Fig. 4*a*

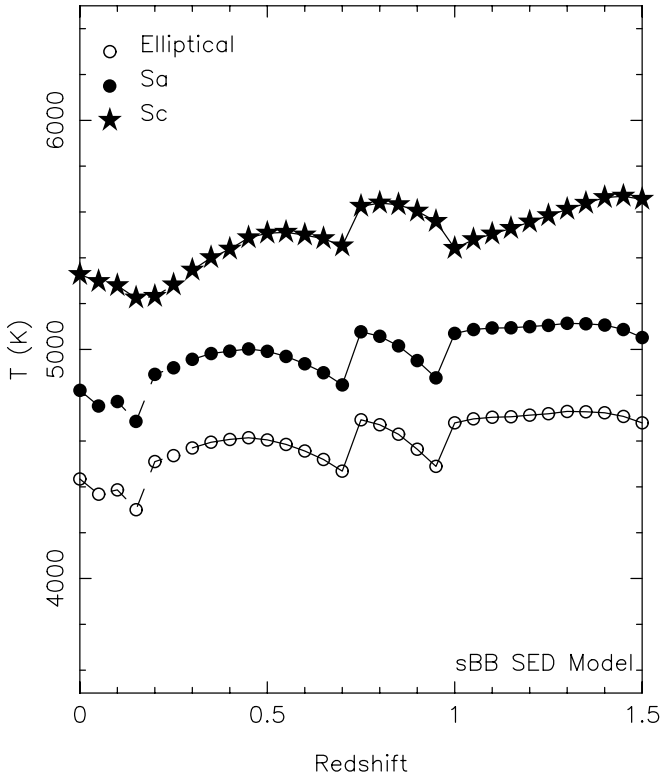

Fig. 4*b*

FIG. 4.—Measured parameters from the sBB model fit shown [α_{UV} in (*a*) and T for the optical and near-IR in (*b*)] for the standard test set of local galaxy SEDs (those of Fig. 1) observed over the range in redshift from 0.0 to 1.5. The plot symbols are the same as those of Fig. 2. The vertical line in (*a*) reminds us that the UV fit is not considered valid in the region of $z < 0.25$.

3.8. *Special Cases*

A number of special cases arose for very faint or very crowded objects in the flanking fields. If there was no detection of a galaxy at 2.2 μ, then the median value of the IR parameter for that redshift range and galaxy spectral type (see § 4) was adopted for the object. A check was made to be sure that this value was consistent with the limit of $K \sim 20$ of the H00 photometric survey and of the somewhat fainter limit for the Barger et al. (1999) survey.

If the object was very crowded, usually the fainter of a close pair on the sky, the H00 database only contains an R mag, which was estimated after the main database was assembled during the cross-checking of the redshift catalog with the photometric catalog (see Cohen et al. 2000 for details). In such cases, the relevant median was adopted for each of the SED parameters. The rest-frame B luminosity was then the only parameter calculated from the limited observations available.

There are a total of 33 such objects. These galaxies are not included in Table 1 nor in any plots of the spectral indexes nor calculations of their properties, but they will be included in calculating the luminosity function in a future paper.

With two exceptions, we were able to determine reliable SEDs for all the galaxies with redshifts within the HDF-N itself.

4. PROPERTIES OF THE SEDs

We discuss the properties of the SEDs as a function of redshift, luminosity, galaxy star formation rate, etc. To demonstrate that the results are robust, we retain both the 2p and the sBB fits in the tables; however, since the sBB model for galaxy SEDs is clearly superior, only those fits are shown in the remaining figures. We use the galaxy spectral classification scheme defined by Cohen et al. (1999b), which basically characterizes the strength of the strongest emission lines, particularly [O II] at 3727 Å, [O III] at 5007 Å, and Hα, relative to the strong absorption features, H and K of Ca II and the normal absorption in the Balmer lines. To review briefly, $\mathscr{E}$ galaxies have spectra dominated by emission lines, $\mathscr{A}$ galaxies have spectra dominated by absorption lines, while $\mathscr{I}$ galaxies are of an intermediate type. Galaxies with broad emission lines are denoted as spectral class $\mathscr{2}$. Starburst galaxies showing the higher Balmer lines (Hγ, Hδ, etc.) in emission are denoted by $\mathscr{B}$, but for such faint objects, it was not always possible to distinguish them from $\mathscr{E}$ galaxies. These classifications were assigned in Paper X (Cohen et al. 2000) for the galaxies of our sample in the region of the HDF-N.

To illustrate our SEDs applied to real galaxies, Figure 6 shows the SEDs for the five sources in the HDF-N detected by *Chandra* (Hornschemeier et al. 2000) included in our sample. The mid-IR luminosities determined from *Infrared Space Observatory* (*ISO*) observations by Aussel et al. (1999) and the Very Large Array (VLA) radio luminosities inferred from the work of Richards et al. (1998) and Richards (2000) are shown as well, when the galaxies were detected. The X-ray detections are in galaxies with spectral classes $\mathscr{2}$ (a broad-lined AGN), $\mathscr{A}$, $\mathscr{I}$, $\mathscr{E}\mathscr{I}$, and $\mathscr{E}$, i.e., three of the five do not show strong narrow emission lines, hence they do not show evidence for a high current rate of star formation.

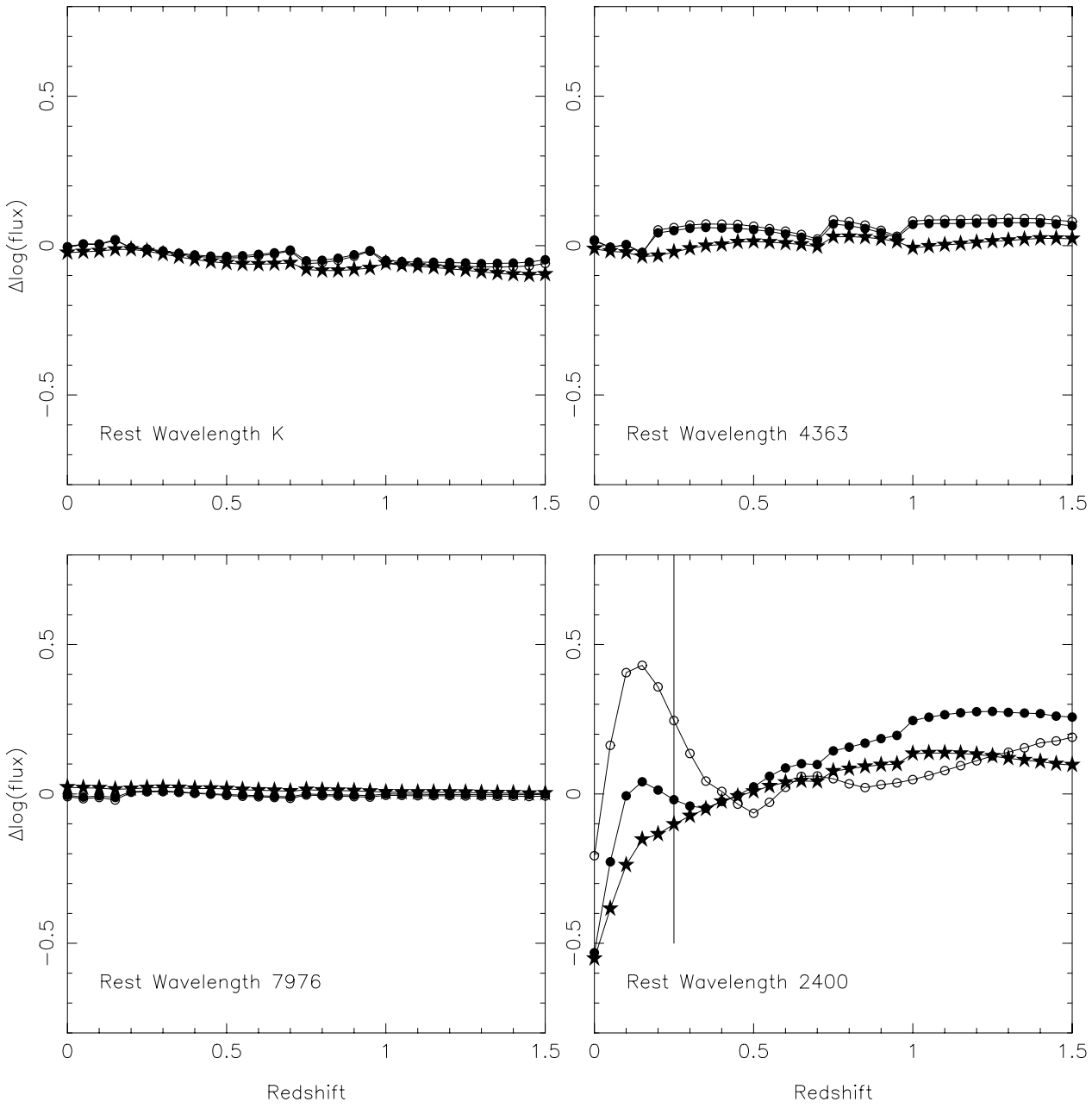

FIG. 5.—Rest-frame galaxy luminosity $L(\nu_0)$ predicted by the best-fit sBB SED model is compared with the actual luminosity of the galaxy SED for the set of standard local galaxy SED models observed over the range in redshift from 0 to 1.5. The plot symbols are the same as those of Fig. 3. The four panels give the results for four different rest wavelengths and are identical in wavelength and scale to the panels of Fig. 3.

4.1. *Correlation between SED Parameters and Galaxy Spectral Types*

Table 2 gives the medians of α_{UV} and α_{IR} from the 2p model SED over the four redshift ranges and for various spectral classes of galaxies. Table 3 provides the same for the parameters α_{UV} and T from the sBB model ($\log T$ is actually used). Only galaxies with reliable redshifts (redshift quality class 1, 2, 4, or 6; see Cohen et al. 1999b for definitions) are used, as is true for all subsequent tables and figures.[5] While the distribution of these indexes is non-Gaussian, we have used the first and last quartiles of the distribution in each case to produce a corresponding σ, assuming a Gaussian distribution prevails.

The dispersion for each galaxy spectral type is a combination of the intrinsic dispersion and that induced by variations in internal reddening from galaxy to galaxy, as well as the known uncertainties in determining the SED parameters. Making the absurd assumption that the first and last factors are negligible, these values of σ can be used to set firm upper limits on internal reddening variations within galaxies. If one assumes a Galactic extinction law, then $\sigma(A_V) \sim 1$ mag will reproduce the observed range in α_{IR} for each of the three galaxy spectral classes. Again, assuming a Galactic extinction law, the dispersion in

[5] Unless otherwise specified, starbursts (galaxy spectral type $\mathscr{B}$) are included with the $\mathscr{E}$ galaxies. Broad-lined AGNs are excluded throughout.

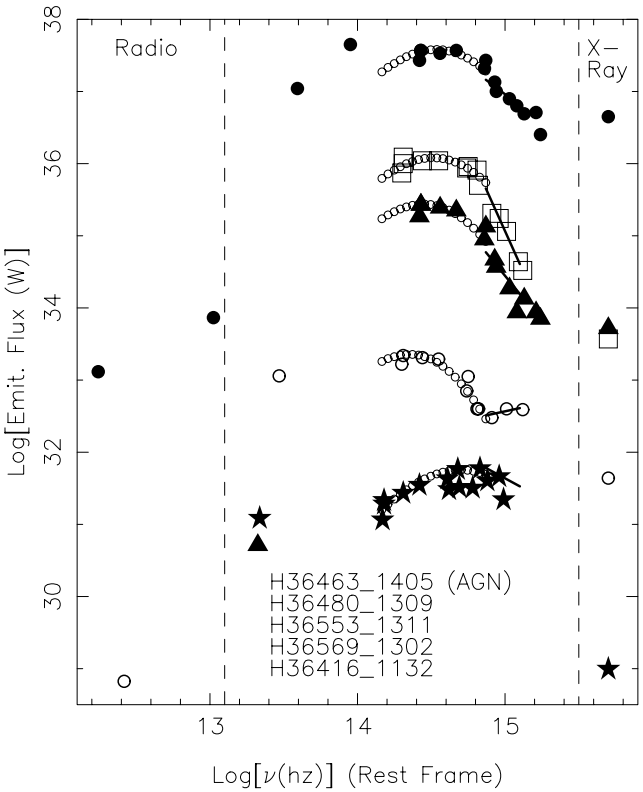

FIG. 6.—SEDs for the five galaxies in the HDF-N in our sample, with detections in the X-ray by *Chandra* from Hornschemeir et al. (2000) included. The sBB fits are shown, as well as the mid-IR detections from *ISO* of Aussel et al. (1999) and the VLA radio detections of Richards et al. (1998) and Richards (2000) at 1.4 and 8.5 GHz. The frequency scale is correct for the optical and mid-IR but is discontinuous at each end to include the radio and X-ray detections. The vertical scale is correct for the uppermost galaxy (H36463_1405) shown. A vertical shift of 1 dex downward is applied for each additional galaxy plotted. The vertical order of the galaxies in the optical is that given in the text insert at the bottom of the figure.

reddening required to reproduce the range of α_{UV} is about one-third as large. The adoption of a grayer reddening curve will allow a larger range in A_V.

As expected, the galaxy spectral classes are correlated with the overall SED shape. "Bluer" galaxies (those with bluer continua) tend to have stronger emission lines, while redder galaxies tend not to have detectable emission lines. This is apparent in the local universe, and we reaffirm this again at much higher redshifts. This is true not only for the rest-frame UV continuum, but also for the rest-frame Paschen continuum, although the effect is smaller there. The observation that galaxies with strong emission lines (i.e., those with strong current star formation) are bluer is one found by many other surveys, both locally and within the redshift range under discussion here, e.g., Lin et al. (1996) for the Las Campanas Redshift Survey, Ellis et al. (1996) for the Low-Dispersion Survey Spectrograph redshift survey, and Cowie et al. (1996) and Hammer et al. (1997) for the Canada-France Redshift Survey (CFRS).

Figure 7 shows a plot of the two sBB SED parameters, α_{UV} and T, for galaxies in the mid- and high-redshift ranges. This figure (when constructed using the 2p SED model parameters) looks very similar to the corresponding figure (Fig. 5), given in Cohen et al. (1999a), of the data analysis from our survey field at J0053+1234. As would be expected from Tables 2 and 3, galaxies whose spectra are dominated by emission lines occupy a different area in this plot than do the galaxies without detectable emission lines. Again as expected, galaxies with strong emission lines are significantly bluer in the rest-frame UV and somewhat bluer in the rest-frame optical/near-IR, while galaxies with no sign of ongoing star formation are redder in both the rest-frame UV and Paschen continuum.

To reinforce this point, a histogram of SED indexes with galaxy spectral type for galaxies in the mid- and high-redshift range is shown in Figures 8*a* and 8*b*.

TABLE 2

MEDIAN SPECTRAL INDEXES FOR OBJECTS IN THE REGION OF THE HDF-N USING THE 2P SED MODEL

		α_{UV} [a]			α_{IR} [a]		
RANGE	NUMBER	*A*	*I*	*E*	*A*	*I*	*E*
$0.25 < z < 0.5$.....	155	4.5 (0.6)	2.6 (0.1)	1.8 (0.1)	1.0 (0.1)	1.0 (0.1)	0.6 (0.1)
$0.5 < z < 0.8$	199	5.3 (0.2)	2.6 (0.1)	1.4 (0.1)	1.4 (0.1)	1.2 (0.1)	0.6 (0.1)
$0.8 < z < 1.05$.....	135	5.1 (0.7)	2.8 (0.3)	1.3 (0.1)	1.3 (0.1)	1.3 (0.1)	0.8 (0.1)
$1.05 < z < 1.5$.....	26	5.3 (1.0)	...	1.1 (0.2)	1.3 (0.2)	...	1.1 (0.1)

[a] All entries have the median followed in parentheses by the 1 σ uncertainty of the median calculated assuming Gaussian statistics hold.

TABLE 3

MEDIAN SPECTRAL INDEXES FOR OBJECTS IN THE REGION OF THE HDF-N USING THE SBB SED MODEL

		α_{UV} [a]			T [a]		
RANGE	NUMBER	*A*	*I*	*E*	*A*	*I*	*E*
$0.25 < z < 0.5$.....	155	4.4 (0.7)	2.2 (0.1)	1.4 (0.1)	5125 (100)	5400 (100)	6575 (100)
$0.5 < z < 0.8$	199	4.8 (0.3)	1.9 (0.1)	1.0 (0.1)	4875 (100)	5300 (100)	6600 (100)
$0.8 < z < 1.05$.....	135	4.7 (0.6)	2.8 (0.3)	1.0 (0.1)	4900 (100)	4950 (100)	6700 (100)
$1.05 < z < 1.5$.....	26	4.3 (1.0)	...	0.7 (0.2)	4600 (300)	...	6100 (200)

[a] All entries have the median followed in parentheses by the 1 σ uncertainty of the median calculated assuming Gaussian statistics hold.

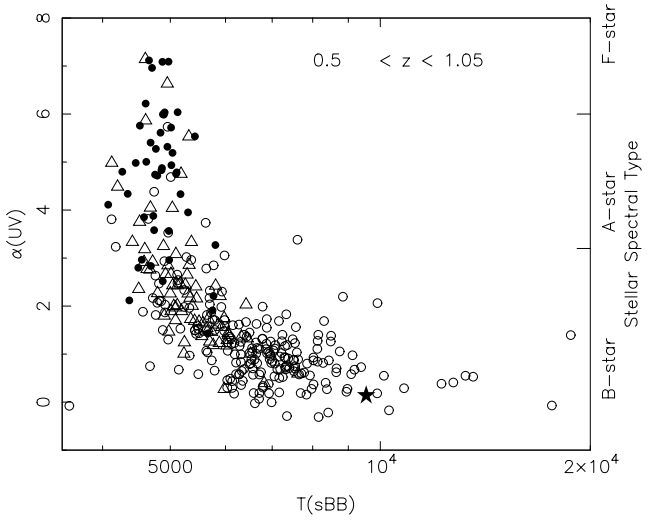

FIG. 7.—Spectral indexes α_{UV} shown as a function of log T for galaxies in the region of the HDF-N in the mid- and high-redshift ranges. Filled circles denote galaxies of spectral type $\mathscr{A}$, triangles denote galaxies of spectral type $\mathscr{I}$, and open circles denote galaxies with strong emission lines (spectral type $\mathscr{E}$). Starbursts (spectral type $\mathscr{B}$) are denoted by stars. Note that only the first letter of the galaxy spectral class is used. The range of α_{UV} for stars of various spectral types, taken from Cohen et al. (1999a), is shown on the right side of the figure.

4.2. *Correlation between SED Parameters and Redshift*

Tables 2 and 3 demonstrate a decrease of α_{UV} with increasing redshift for $\mathscr{E}$ galaxies, which is in the expected sense, i.e., higher redshift star-forming galaxies appear bluer in the rest-frame UV than their local counterparts probably because of a higher contribution to the total galaxy luminosity from young stars, in other words, a higher mean star formation rate per unit galaxy luminosity. One may also attribute this change to the limited ability of even the sBB model to produce, for a fixed galaxy SED, a constant value of α_{UV} as a function of redshift (see Fig. 4).

However, with the exception noted above, the UV and optical/near-IR SED indexes (α_{UV} and α_{IR} or T) appear to be constant with redshift for each of the three major galaxy spectral classes, $\mathscr{A}$, $\mathscr{I}$, and $\mathscr{E}$, to within the uncertainties defined by assuming that the scatter has a Gaussian distribution for the low, mid, and high spectral ranges. The CFRS group (Hammer et al. 1997) also found only modest evolution in mean colors with redshift.

The rest-frame optical/near-IR continua of $\mathscr{E}$ galaxies appear to become somewhat redder at high redshifts, but this is dependent on the median of T or α_{IR} for the highest redshift bin. It is not surprising that the $\mathscr{E}$ galaxies in the highest redshift range appear to have somewhat redder rest-frame optical continua, since at that point the galaxy spectral classification becomes unreliable, and the $\mathscr{E}$ class is a catchall for a wide range of galaxies. Similar concerns manifest themselves for the highest z range in which I galaxies could be detected.

This result is equivalent to stating that the association between the spectral indexes that characterize the continuum slopes of the median rest-frame SED of galaxies and the presence of certain discrete narrow spectral features (i.e., those that define the galaxy spectral classes $\mathscr{A}$, $\mathscr{I}$, and $\mathscr{E}$) are roughly invariant out to $z \sim 1.1$, with the exception that actively star-forming galaxies become bluer in the UV at higher redshifts.

We can compare the behavior of the SED parameters with redshift with that predicted by Poggianti's (1997) galaxy evolutionary synthesis models. We apply the same procedure to determine the power-law indices to these galaxy models, assuming that her E, Sa, and Sc models correspond roughly to our galaxy spectral classes $\mathscr{A}$, $\mathscr{I}$, and $\mathscr{E}$. Her elliptical models show SEDs that change little with age, at least to $z \sim 1$, in accordance with the data shown in Table 2. This corresponds to the well-known diffi-

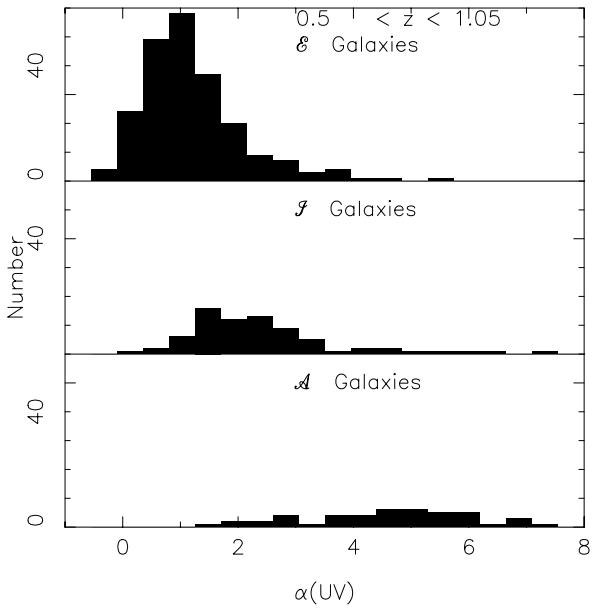

Fig. 8*a*

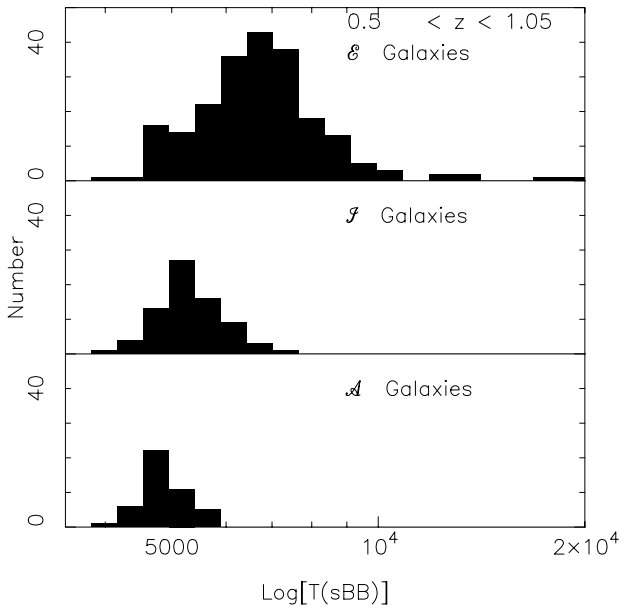

Fig. 8*b*

FIG. 8.—Histograms of the spectral indexes α_{UV} and T(sBB) are shown in (*a*) and (*b*) for galaxies of spectral classes $\mathscr{A}$, $\mathscr{I}$, and $\mathscr{E}$ in the mid- and high-redshift ranges. Note that only the first letter of the galaxy spectral class is used.

TABLE 4

MEDIAN R LUMINOSITY AS A FUNCTION OF SPECTRAL INDEX FOR OBJECTS IN THE REGION OF THE HDF-N (2P SED MODEL)

α_{UV}			α_{IR}		
Range	Number	$\log L(R)$[a] (W)	Range	Number	$\log L(R)$[a] (W)
$0.25 \leq z < 0.5$					
0–1	9	35.50 (0.1)	−2 to −1	0	…
1–2	50	35.83 (0.1)	−1 to 0	14	35.47 (0.1)
2–3	48	36.11 (0.1)	0–1	83	35.98 (0.1)
3–4	27	36.25 (0.1)	1–2	53	36.38 (0.1)
4–5	12	36.64 (0.1)	2–3	5	35.77 (0.2)
5–6	5	36.60 (0.1)	4–5	0	…
$0.5 \leq z < 0.8$					
0–1	17	35.85 (0.1)	−2 to −1	0	…
1–2	75	36.32 (0.1)	−1 to 0	6	35.63 (0.1)
2–3	59	36.47 (0.1)	0–1	109	36.29 (0.1)
3–4	16	36.75 (0.1)	1–2	84	36.79 (0.1)
4–5	10	36.81 (0.1)	2–3	0	…
5–6	13	36.69 (0.1)	4–5	0	…
$0.8 \leq z < 1.05$					
0–1	34	36.46 (0.1)	−2 to −1	0	…
1–2	55	36.65 (0.1)	−1 to 0	4	36.27 (0.1)
2–3	21	36.91 (0.1)	0–1	65	36.57 (0.1)
3–4	11	37.02 (0.1)	1–2	63	36.99 (0.1)
4–5	3	37.06 (0.2)	2–3	4	36.90 (0.1)
5–6	7	37.15 (0.1)	4–5	0	…
$1.05 \leq z < 1.5$					
0–1	11	36.47 (0.1)	−2 to −1	1	37.03 (…)
1–2	10	36.86 (0.1)	−1 to 0	2	36.65 (0.1)
2–3	3	36.66 (0.2)	0–1	5	36.34 (0.2)
3–4	0	…	1–2	15	36.91 (0.1)
4–5	1	37.41 (…)	2–3	3	36.68 (0.2)
5–6	0	…	4–5	0	…

[a] All entries have the median followed in parentheses by the 1 σ uncertainty in the median computed assuming Gaussian statistics apply.

culty of determining the age of an old stellar population from broadband photometry alone.

However, Poggianti's Sa and Sc models become bluer at all wavelengths within the range of interest more rapidly between $z \sim 0$ and ~ 1 than do the galaxy SEDs in our sample. This difference is significantly larger than the uncertainties.

Galaxy evolutionary synthesis calculations involve many theoretical inputs and many assumptions, with only a limited number of constraints applying, mostly at $z = 0$. One expects that the errors in stellar evolutionary tracks or in our cosmology (i.e., in the relationship between redshift and age) will not be substantial. However, errors in the synthesis models arising from the forms adopted for the star formation rate as a function of time (i.e., at $z > 0.5$) for the various current galaxy spectral classes may be more serious.

An interesting possibility for a partial explanation is a scenario in which as galaxies evolve in time, their SEDs age, and their morphological classifications also evolve. Van den Bergh et al. (2000), among others, present evidence from an analysis of the morphology of this sample of galaxies on the HDF-N images taken by *HST*, supporting morphological evolution of galaxies with redshift.

The most likely explanation of this difference between the behavior with redshift of the SED parameters of our sample, divided in spectral classes, and the predictions of galaxy evolution models is that the star formation rate of a particular model galaxy from Poggianti (1997) varies so much with time out to $z \sim 1.5$ that, as their SEDs age, the galaxies will shift between the relatively small number of galaxy spectral classes used here. This is an issue that will be explored in future work.

4.3. *Correlation of Luminosity with Color*

In Cohen et al. (1999a), we found a tentative relationship between spectral slopes and galaxy luminosity such that more luminous galaxies are redder, suggestive of a continued correspondence at high z to the well-known galaxy luminosity–mean metallicity relationship shown by early-type galaxies in the local universe (see, e.g., the discussion of spiral galaxies in Zaritsky, Kennicutt, & Huchra 1994; for the dwarf galaxies in the Local Group, see Côté, Oke, & Cohen 1999). The large range in star formation rates among galaxies will also contribute to a relationship between star formation rate and luminosity, if most star formation is now occurring within low-luminosity galaxies. Such galaxies

TABLE 5

MEDIAN BLUE LUMINOSITY AS A FUNCTION OF SPECTRAL INDEX FOR OBJECTS IN THE REGION OF THE HDF-N (sBB MODEL)

α_{UV}			T(sBB)		
Range	Number	log $L(\lambda_m$, red)[a] (W)	Range	Number	log $L(\lambda_m$, red)[a] (W)
		$0.25 \leq z < 0.5$			
−1 to 0	1	35.14 (...)	3800–4375	8	35.89 (0.2)
0–1	29	35.76 (0.1)	4375–5025	26	36.47 (0.1)
1–2	59	36.04 (0.1)	5025–5775	42	36.24 (0.1)
2–3	36	36.14 (0.1)	5775–6650	33	36.03 (0.1)
3–4	17	36.30 (0.1)	6650–7650	28	35.78 (0.1)
4–5	5	36.39 (0.1)	7650–8800	7	35.62 (0.1)
5–6	6	36.51 (0.2)	8800–10125	4	35.47 (0.1)
		$0.5 \leq z < 0.8$			
−1 to 0	5	35.76 (0.1)	3800–4375	5	36.65 (0.1)
0–1	52	36.21 (0.1)	4375–5025	39	36.74 (0.1)
1–2	67	36.46 (0.1)	5025–5775	52	36.51 (0.1)
2–3	36	36.56 (0.1)	5775–6650	50	36.29 (0.1)
3–4	11	36.52 (0.2)	6650–7650	35	36.38 (0.1)
4–5	14	36.54 (0.1)	7650–8800	10	36.15 (0.1)
5–6	9	36.67 (0.1)	8800–10125	5	36.19 (0.2)
6–10	4	36.74 (0.1)			
		$0.8 \leq z < 1.05$			
−1 to 0	3	35.87 (0.1)	3800–4375	3	36.61 (0.1)
0–1	49	36.56 (0.1)	4375–5025	31	36.92 (0.1)
1–2	45	36.72 (0.1)	5025–5775	22	36.87 (0.1)
2–3	17	36.73 (0.1)	5775–6650	20	36.30 (0.1)
3–4	9	36.75 (0.1)	6650–7650	33	36.63 (0.1)
4–5	5	36.92 (0.1)	7650–8800	16	36.59 (0.1)
5–6	5	36.92 (0.1)	8800–10125	6	36.49 (0.2)
6–10	5	37.01 (0.1)	>10125	6	36.51 (0.2)
		$1.05 \leq z < 1.5$			
−1 to 0	1	36.51 (...)	3800–4375	0	...
0–1	13	36.69 (0.1)	4375–5025	5	36.96 (0.2)
1–2	8	36.96 (0.1)	5025–5775	4	36.64 (0.1)
2–3	3	36.57 (0.1)	5775–6650	7	36.77 (0.2)
3–4	0	...	6650–7650	7	36.58 (0.2)
4–5	0	...	7650–8800	1	37.39 (...)
5–6	0	...	8800–10125	0	...
6–10	1	37.52 (...)	>10125	3	36.51 (0.1)

[a] All entries have the median followed in parentheses by the 1 σ uncertainty in the median computed assuming Gaussian statistics apply.

would then appear bluer than high-luminosity, more quiescent galaxies (see, e.g., Boselli et al. 2001).

We now examine our much larger data set in the HDF-N to see if this trend persists. We construct the rest-frame optical luminosity using the parameters from the SED fit for each galaxy. For the 2p SED model, we use rest-frame R, while for the sBB model, we use $L(\lambda_m$, red). Even for the highest redshift galaxies in this sample, rest-frame R lies within the range of the existing broadband photometry, so no extrapolation of the SED is required.

The results are given in Table 4 for the 2p SED model and in Table 5 for the sBB SED model. The luminosity characteristic of each redshift range rises with increasing z, as is expected, since ours is a magnitude-limited sample. There is a clear trend of galaxies with redder UV power-law indices (larger α_{UV}) being more luminous in every redshift range except in the highest range (see Fig. 9). The increase in median rest-frame optical luminosity from the bluest to the reddest galaxies in each redshift range is about a factor of 5.

The same trend is present for the IR power-law indices, but the increase is by a smaller factor, about 3, from the bluest to the reddest galaxies.

The highest redshift range behaves anomalously, but that is not surprising, since only the most luminous galaxies can be detected there at such high redshifts, and the depth in luminosity of the sample is small. Furthermore, it is very difficult to assign redshifts beyond $z \sim 1$ to systems dominated by strong absorption lines, which are the most luminous galaxies in the lower redshift ranges; any such galaxies may be so red as to fall below the R cutoff of our sample.

To summarize, the reddest galaxies in both the rest-frame UV and optical/near-IR tend to be the most luminous, at least to $z = 1.05$, after which such a trend, if present, would be very hard to establish from our sample. For example, of

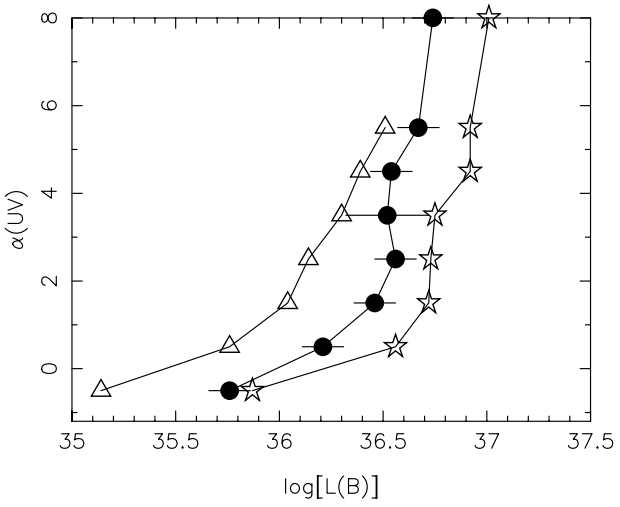

FIG. 9.—Relationship between the median luminosity $L(B)$ in bins of rest-frame UV and spectral slope α_{UV} shown as a function of redshift for three of the four redshift bins. (The highest redshift bin is not shown.) The open triangles denote the sample of galaxies in the region of the HDF-N with $0.25 < z < 0.5$, the filled circles denote galaxies with $0.5 < z < 0.8$, and the open stars denote galaxies with $0.9 < z < 1.05$. The range in luminosity within a given bin in UV spectral slope is indicated by the $\pm 1\ \sigma$ horizontal bars displayed for the second redshift range only. More luminous galaxies are seen to be redder in the rest-frame UV.

the 25 most luminous (in rest-frame R) galaxies with $0.25 < z < 0.8$, 12 have been assigned to galaxy spectral class $\mathscr{A}$, but less than 15% of the total sample within that redshift range is assigned to this spectral class.

This is a well-established trend in the local universe, shown clearly in the recent large samples from the SDSS and 2dF surveys analyzed by Blanton et al. (2001) and Folkes et al. (1999), respectively.

Since this is true in the rest-frame optical, the effect will be even larger at rest-frame K, which is a better measure of the true luminosity of the stellar system, unperturbed by contributions from a small number of bright young (blue) stars.

We thus see a picture of quiescent non–star-forming galaxies being the most luminous at each z, while star-forming galaxies are bluer and also have, on average, significantly lower rest-frame optical (and even more so, K) luminosities in each of the redshift ranges up to $z \sim 1.1$.

5. PROPERTIES OF THE SEDs OF THE $\mathscr{E}$ GALAXIES

Our selection of star-forming galaxies is complete, in that all objects with strong emission lines are included in the $\mathscr{E}$ spectral class. We would see strong emission lines, if such were present, in any galaxy of *any* spectral slope with $z < 1.2$,[6] if that galaxy fell within our magnitude-limited survey.

5.1. *UV SEDs of Starburst Galaxies from $z \sim 0$ to ~ 3*

Calzetti, Kinney, & Storchi-Bergmann (1994), in their study of local starburst galaxies, define the UV extinction in terms of the spectral power-law index β derived for f_λ, where in terms of our UV index α_{UV}, $\beta = \alpha_{UV} - 2.0$. Their latest calibration of β versus $E(B-V)$ and versus absorption at 1600 Å is given in Meurer, Heckman, & Calzetti (1999). Their data demonstrate that local starbursts have $-0.5 < \alpha_{UV} < +2.5$, with a median of ~ 0.6.

There are too few spectroscopically identified starbursts in our sample to examine their SED properties.[7] Instead, we consider the SED properties of the entire population of $\mathscr{E}$ galaxies. Figure 8*a* shows that for the mid- and high-redshift group (as is true also of the other two redshift groups), there is a falloff on the blue side of the distribution of α_{UV} at a value of ~ 0.6. Moreover, both Steidel et al. (1999) and Meurer et al. (1999) find for U dropouts at $z \sim 3$ about the same median β of -1.6 (corresponding to $\alpha_{UV} = +0.6$), and they deduce from this a median of $E(B-V) \approx 0.15$ mag.

While this result was anticipated and is therefore not a surprise, it is by no means one that is guaranteed. The mean starburst SED is not as blue as that of the hottest known stars, but rather represents a sum over a population, including some very hot stars. There is no reason beyond our perception of what is logical why a very young galaxy could not have an even bluer UV SED, as do a very small number of local galaxies whose UV light may be dominated by the contribution of a few Wolf-Rayet stars (Sullivan et al. 2000; Brown et al. 2000). The bluest possible galaxy SED would be the Rayleigh-Jeans tail of a population of very hot stars, with $\alpha_{UV} = -2.0$, much bluer than that of observed galaxies. The mass of the highest mass star in a young population and the nature of the UV SED from a starburst has been studied theoretically by Elmegreen (2000). He derives colors considerably bluer than observed starburst colors and is forced to introduce a mechanism to produce a cutoff in the upper mass below that expected.

We thus find strong evidence that the most extreme starburst galaxies (i.e., the bluest galaxies in the rest-frame UV) have indistinguishable SEDs in the rest-frame UV over the entire redshift range $0 < z < 3$.

5.2. *On the Existence of Highly Reddened Starbursts in Our Sample*

We now turn to the nature of the far-IR objects observed in the submillimeter regime by SCUBA (Blain et al. 1999; Smail et al. 1999; Lilly et al. 1999; for the HDF-N, Hughes et al. 1998) and their relationship to the galaxy populations normally studied at optical wavelengths. We use our SEDs to explore the issue of whether these galaxies might be some tail of the optically detected galaxy population with unusually high internal reddening. Smail et al. (1999), Richards et al. (1999), and Barger, Cowie, & Richards (2000), among others, have suggested that these far-IR sources represent the tip of a vast iceberg of a separate population of very dusty galaxies at high z, in which an enormous amount of star formation is occurring and which are invisible at optical wavelengths. Are these SCUBA sources closer to the ultraluminous infrared galaxies (ULIRGs) reviewed by Sanders & Mirabel (1996) or to the redder of the Lyman break galaxies already observed at

[6] At $z > 1.2$, the 3727 Å emission line of [O II] is shifted to 8200 Å, where the night-sky emission is becoming fierce. At $z > 1.5$, the line is shifted to the point at which the quantum efficiency of most CCD detectors is rapidly declining.

[7] Ignoring the starburst galaxy at $z = 0.137$, whose UV spectral index is not reliably determined, the five starbursts spectroscopically identified as such in our sample have a very wide range in α_{UV} from 0.1 to 2.7, with a very poorly determined median α_{UV} of 0.6.

optical wavelengths, as suggested by Adelberger & Steidel (2000)? Do their presence and numbers imply that it is "useless" to study galaxies in the optical?

Assuming SCUBA sources are not AGNs, but rather dusty starbursts, we attempt to isolate galaxies from our sample with a high rate of ongoing star formation most comparable with the galaxies detected with SCUBA. We take the group of galaxies with strong emission lines, i.e., those classified as $\mathscr{E}$, as the relevant sample, recognizing that this is a somewhat more diverse group that may contain many galaxies "older" and with less current star formation than those detected by SCUBA or than pure local starburst galaxies. Hence, the intrinsic UV power-law index of many of these galaxies may be somewhat redder than that of a pure starburst.

Figure 8*a* suggests for strong emission-line galaxies in our sample a continuous distribution of α_{UV}, peaked at a level slightly redder than that of local starbursts and of $z \sim 3$ *U* dropouts. There is no obvious second (redder) component, although there may be an extended low-level red tail to the distribution. One should note, however, that the distribution in α_{UV} shown in Figure 8*a* for the $\mathscr{E}$ galaxies includes both $\mathscr{E}$ and $\mathscr{E}\mathscr{I}$ galaxies.[8] When restricted to just $\mathscr{E}$ galaxies, the red tail is reduced relative to the blue peak. Furthermore, galaxies in the red tail of this distribution do not seem to have lower luminosities, as would be expected were the red tail due primarily to internal reddening.

This whole issue is related to the nature of the extremely red objects found in deep IR selected samples. As we have stated earlier (Cohen et al. 1999a, 2000; see also Scodeggio & Silva 2000), evidence from our redshift surveys suggests that the majority of the EROs in this magnitude regime with $R - K \sim 5$–6 are passively evolving "old" stellar populations at $z \sim 1.3$. While there are undoubtedly some very red, very dusty ULIRGs with extensive star formation similar to the ERO HR 10 at $z = 1.44$ (Dey et al. 1999 and references therein), these appear to be rare.

Our analysis of the SEDs of galaxies with strong emission lines in our *R*-selected sample does not provide any evidence that supports the existence of a significant "missed" population of dusty galaxies with extensive star formation that might be forming a significant fraction of the stars in the universe within the regime $z \lesssim 1.5$. Dust enshrouded starburst nuclei that do not dominate the total integrated light from a distant galaxy cannot be excluded by our SEDs. However, Moriondo, Cimatti, & Daddi (2000) and Stiavelli & Treu (2000) find that *HST* images of EROs are extremely red not just within the nucleus, but over the entire galaxy image.

5.3. *Prediction of the Mid-IR Flux from the UV Spectral Index*

Meurer et al. (1999) have provided a formalism for predicting the far-IR thermal dust emission from the UV spectral indexes of starbursts. They suggest that as the amount of dust increases, the UV spectral index becomes redder and deviates further from the extremely blue power-law index characteristic of bare young starbursts. The absorbed UV radiation is then reemitted by dust in the mid- and far-IR. Meurer et al. (1999) give the relevant relationships calibrated by their analysis of local starbursts to predict the emitted flux in the thermal-IR from dust.

We attempt to use their formalism to predict which of the galaxies in the region of the HDF-N should have been detected in the mid-IR by *ISO*, assuming that a correlation between mid- and far-IR emission exists. We employ a ranking scheme to do this, comparing the list of galaxies actually detected by *ISO*, from the analysis of Aussel et al. (1999), with our entire sample. The optical counterparts of the *ISO* galaxies are discussed and listed in Cohen et al. (2000). Only those with $R < 22.8$ (i.e., those for which the identification is considered reasonably certain) are included. Since the *ISO* optical counterparts are of spectral type $\mathscr{E}$, $\mathscr{E}\mathscr{I}$, or $\mathscr{E}\mathscr{A}$ (Cohen et al. 2000), we also predict the mid-IR flux for the galaxies within our sample of those spectral types (as well as the spectroscopically identified starbursts, which are mostly of too low a luminosity to have been detected by *ISO*) and with $R < 22.8$.

Because of the correlation between galaxy spectral type and SED indexes shown in Tables 2 and 3 and Figure 8, a misclassification of a galaxy to spectral type $\mathscr{E}$ that is actually an intermediate spectral type ($\mathscr{I}$, $\mathscr{E}\mathscr{I}$, or $\mathscr{I}\mathscr{E}$), will produce a galaxy that appears slightly too red in the rest-frame UV, hence seems excessively dusty. The predicted mid-IR flux for such a misclassified object will be overestimated. This type of classification error should not occur until a galaxy is either very faint or has $z > 0.9$, where the 4000 Å region is shifted into the thicket of night-sky lines, and it is very hard to distinguish anything except the emission features. Hence, the mid-IR luminosity prediction is carried out for the redshift range of 0.25–1.05, omitting the highest *z* range, in which the galaxy spectral types are more uncertain.

There are 12 *ISO* galaxies with secure optical counterparts in the relevant redshift range. We find the ranking of the 12 *ISO* galaxies in predicted mid-IR luminosity using the formalism of Muerer et al. within the set of 154 potential optical counterparts from our survey selected as described above. For comparison, we ascertain the rank of the *ISO* galaxies in the total sample when ordered by $L(B)$ or $L(R)$.

Figure 10 shows the rankings of the 12 *ISO*-detected galaxies in this redshift range within the sample of 154 galaxies. A perfect discriminant would have the *ISO* galaxies occupying ranks 1–12. None of the discriminants tried is very good. The results are unchanged when only $\mathscr{E}$ galaxies are used. They are also unchanged when a correction to the luminosity for passive evolution is made. The sBB SED model fits were used throughout; the results are unchanged when the 2p fits are used.

The best discriminant appears to be the *B*-band luminosity. The mid-IR flux predicted with the algorithm of Meurer et al. (1999) for the galaxies detected by *ISO* in our sample does not appear to do better overall than either the *B*- or *R*-band luminosity. While the *ISO* detections correspond to galaxies that are among the most luminous (using any of the three definitions of luminosity given above), there are still many galaxies of comparable luminosity that were not detected by *ISO*. The formalism of Meurer et al. (1999) does not significantly reduce this problem. One should note, however, that this formalism was developed to explain the far-IR emission of galaxies where thermal emission from dust dominates. At a typical redshift of 0.6, the 15 μ *ISO* bandpass corresponds to 9.4 μ in the rest frame.

[8] Unless otherwise specified, throughout this paper, a galaxy's spectral class for purposes of plots and figures is defined only by the first character of its assigned spectral class.

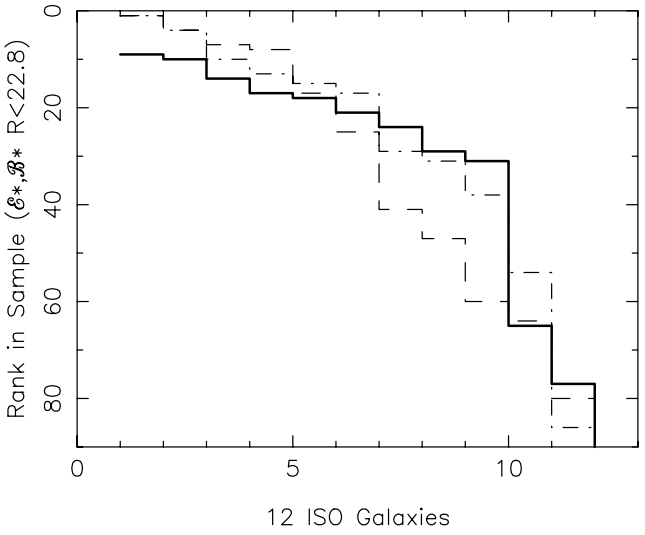

FIG. 10.—Ranking of the galaxies detected by *ISO* within the sample of all (154) galaxies, with spectra showing strong emission lines and $R < 22.8$, shown for the redshift range $0.25 < z < 1.05$. The solid line indicates the ranking of the *ISO* galaxies within the sample using $L(B)$, the dashed line is for $L(R)$, and the dot-dashed line uses the mid-IR luminosity predicted using the formalism of Meurer et al. (1999).

6. COMMENTS ON PHOTOMETRIC REDSHIFTS

Photometric redshifts have become very popular recently (see, e.g., Connolly et al. 1997; Fernández-Soto et al. 1999). As our blind tests (Hogg et al. 1998a; Cohen et al. 2000) have shown, these are capable of accurately predicting the true redshift of an object in essentially all cases with the excellent photometry that one can obtain from deep *HST* images. However, many wide-area ground-based surveys plan to use photometric redshifts for various purposes, and one might be concerned that the limitations of ground-based photometry for such faint objects will reduce the accuracy of the resulting photometric redshifts beyond a tolerable level.

There are two problems here, both becoming worse as one presses fainter. The first is the impact of crowding, while the second is the decreasing accuracy of the photometry itself for isolated fainter objects. We can assess the influence of the former in that even with very careful hand checking of all objects in our sample in the region of the HDF-N and with images with 1″ seeing, we could not obtain believable SEDs for about 25 of 590 objects because of crowding.[9] Almost all these objects have $R > 22$. That error rate in a massive nonmanually checked catalog at this magnitude level would be larger and would further increase by a large factor for a catalog with a fainter limiting magnitude or poorer seeing conditions. The influence of confusion on photometry is discussed by Hogg (2001). Even in the HDF-N itself, our survey still operates at a level in excess of 60 resolution elements per source.

The 4000 Å break is the dominant feature in the spectra of galaxies in this redshift range.[10] If the photometric errors are such that it is impossible to discern the presence of the break, assignment of a photo-z becomes problematic at best.

We can test with each of our two fitting models whether a 4000 Å break is measurable. In the case of the 2p SED model, we require that we can detect $\alpha_{\rm IR} - \alpha_{\rm UV}$, which is a broadband change in continuum slope, as nonzero, while the sBB model permits direct measurement of the 4000 Å break.

Our criterion for detectability for the 4000 Å break in the sBB SED model is that $L(\lambda_m, \text{red}) - L(\lambda_m, \text{blue}) \geq 0.05$ dex (corresponding to a 4000 Å break of ≥ 0.13 mag). For the 2p model, we require that $|(\alpha_{\rm IR} - \alpha_{\rm UV})|/\sigma \geq 1.5$, where σ is determined from the fitting procedure and is based on the observed brightness of the object, the number of filters used to determine the SED, and the redshift of the object.

We find the number of galaxies in each redshift range for which, with the definitions given above, the detection of a 4000 Å break is problematic. This fraction is less than 20% for galaxies with $z < 0.8$, but it rises to more than 30% above $z \sim 0.8$. While the overall fraction of galaxies without detectable 4000 Å breaks is approximately the same for the two SED models, the behavior of galaxies of spectral class $\mathscr{A}$, in particular, depends on the fitting scheme adopted. In the 2p model, essentially all such galaxies have easily detectable breaks, while in the more detailed sBB model, they have small 4000 Å breaks but still display substantial changes in the overall spectral slope between the rest-frame UV and optical. In any case, there is clearly a significant population of galaxies, consisting predominantly of those with strong emission lines, that do not have a detectable 4000 Å break or Balmer jump. For such galaxies, adding IR photometry will not help in providing a valid photometric redshift. Only higher precision photometry, difficult to achieve from the ground for such faint objects, will help.

Brunner, Szalay, & Connolly (2000) have discussed this issue at length, since it affects their study of galaxy clustering, which uses photometric redshifts to divide a pencil beam survey into several redshift shells, thus avoiding the projection integral. Their particular application is eased by the fact that, as shown by Hogg, Cohen, & Blandford (2000), throughout this range in z, most of the clustering signal is from the redder early-type galaxies, which will yield reasonably accurate photo-z's under any appropriate scheme.

7. QUALITATIVE VIEW OF THE EVOLUTION OF $L^*(K)$

We show in Figure 11 the rest-frame K-band luminosity $L(K)$, calculated from the sBB parameters of the SED fits, as a function of cosmological comoving volume. The issue of K-corrections has been avoided through the use of multicolor photometry, spanning a broad wavelength range. However, extrapolation beyond the reddest observations (i.e., trusting the functional form of the model SEDs) is required to obtain rest-frame K magnitudes for galaxies in this sample, with the largest extrapolation required for the highest z galaxies.

[9] The number of galaxies without reliable SEDs given in § 3.8 includes galaxies with no observation at K, as well as those suffering from crowding.

[10] We ignore the higher redshift range in which the Lyman break dominates and in which the decline in flux across the boundary is more than a factor of 10, but the objects are, in general, fainter than the range considered here of $R < 24$.

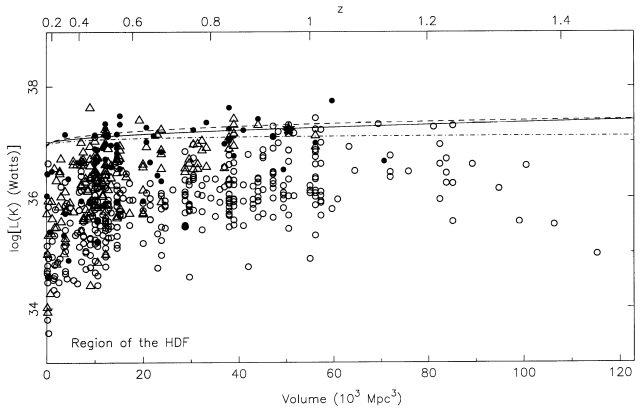

FIG. 11.—$L(K)$ is shown as a function of the cosmological comoving volume for galaxies in the region of the HDF-N with secure redshifts. The plot symbols are the same as in Fig. 7. The lines at the top of the distribution represent the track of a L^* (at K) galaxy with $L = 10^{11}\ L_\odot$ (at $z = 0$) of type E, Sa, and Sc, with evolutionary corrections at K calculated by Poggianti (1997) and applied for $z > 0$.

The rationale for studying galaxies at K is that the integrated light there is much more representative of the total stellar mass of a galaxy than are the optical colors, where light from the most recent epoch of star formation may dominate over that from the older population as one moves toward the ultraviolet. Converting these K luminosities for the galaxies in our sample into total stellar masses of the galaxies requires a model of evolving galaxy SEDs to evaluate their mass-to-light ratio as a function of look-back time and their star formation history. We use the evolutionary corrections from the models of Poggianti (1997), and interpret her E, Sa, and Sc galaxy classes as roughly equivalent to our galaxy spectral types, $\mathscr{A}$, $\mathscr{I}$, and $\mathscr{E}$. The lines in Figure 11 thus indicate the predicted track of a galaxy of constant mass from Poggianti (1997) for the three morphological galaxy classes. As expected, the evolutionary change in luminosity at K predicted by Poggianti (1997) is quite small and much less dependent on the details of the star formation history (i.e., of the galaxy spectral class) than are those predicted at B or R. These tracks, which include passive stellar evolution for the elliptical, are at rest-frame K a good representation of the evolution of at least the most luminous galaxies in our sample.

Recent determinations of $L^*(K)$ in the local universe correspond to $L^*(K) = 8 \times 10^{36}$ W (Gardner et al. 1997; Loveday 1999; from the combination of the 2dF and 2MASS survey, Cole et al. 2001). The passive evolution model lines are shown with this luminosity (at $z = 0$), equivalent to $1.3 \times 10^{11}\ L_\odot$ at K. For elliptical galaxies, using the mass-to-light ratio at K for local ellipticals computed by Worthey (1994), this is a galaxy with a total mass of $1 \times 10^{11}\ M_\odot$. The mass-to-light ratio of Sb galaxies is smaller by about a factor of 2.

Figure 11 suggests, as has been evident from our work on spatial clustering in this field, that luminous nearby ($z \lesssim 0.3$) galaxies are absent in this field. That is presumably a result of the selection criteria for defining the HDF-N adopted by Williams et al. (1996).

Figure 11 also shows the gradual increasing mean luminosity of star-forming galaxies (our spectral class $\mathscr{E}$) to $z \sim 1$ and the increasing dominance of such galaxies as a fraction of the total observed population, an effect found previously with smaller samples by many groups, including Cowie et al. (1996), Hammer et al. (1997), and Hogg et al. (1998b). There are some selection effects, as discussed many times in the earlier papers in this series, namely, faint objects have a lower probability of being assigned a redshift unless they have very strong emission lines, and the same is true for galaxies with $z > 1$. However, the redshift completeness of our sample is very high, in excess of 93%.

A formal analysis of the galaxy luminosity functions will follow in the next paper in this series. Once the evolution of L^* is properly determined, then subject to the accuracy of Poggianti's (1997) predicted evolutionary corrections at rest-frame K and to the uncertainties in the extrapolation of our SEDs beyond the range in wavelength over which photometry exists, one can evaluate the change in the total stellar mass of L^* galaxies. This can then be used to provide another constraint on the rate of massive mergers out to $z \sim 1$; Carlberg et al. (2000) has already provided one such constraint through an analysis of the kinematic pairs in our sample.

8. SUMMARY

In this paper, we have evaluated the SEDs for a sample of 590 galaxies in the region of the HDF-N with $z < 1.5$ using a new versatile and stable SED model. This has been done directly from the data using multicolor photometry with wide wavelength coverage combined with spectroscopic redshifts from our 93% complete R-selected redshift survey here. The behavior of the SEDs with galaxy spectral type (i.e., "recent" star formation history) and with redshift confirms the trends found in our earlier studies of smaller samples; galaxies with strong signs of recent star formation (i.e., those that show emission lines) have bluer continuum slopes in both the rest-frame UV and optical/near-IR. The most luminous galaxies tend to be of the galaxy spectral class $\mathscr{A}$ at a rate much higher than their fraction in the total sample, i.e., the redder galaxies tend to be more luminous. In the mean, actively star-forming galaxies become bluer in the rest-frame UV at higher redshifts, which may perhaps be due to systematic redshift-dependent fitting errors for α_{UV}. We see no other change with redshift in the relationship between SED characteristics and galaxy spectral type defined by the presence and strength of narrow emission and absorption features to $z \sim 1.1$.

We use these SEDs to evaluate the potential accuracy of photometric redshifts, bearing in mind that a break at 4000 Å must be detectable to within the errors of the photometry to assign a photo-z for galaxies in this redshift regime. We also use them to demonstrate that the SEDs in the rest-frame UV of the most extreme starburst galaxies (i.e., the bluest $\mathscr{E}$ galaxies) are indistinguishable SEDs from those of local starbursts, as analyzed by Calzetti et al. (1994), and from those of the Lyman break galaxies at $z \sim 3$ studied by Steidel et al. (1999) and Meurer et al. (1999).

We also attempt to set constraints on the possible existence of a separate class of dusty starburst galaxies and on the variation from galaxy to galaxy within a galaxy spectral class of internal reddening using these SED indexes. Finally, we use the UV spectral indexes of all the strong emission-line galaxies to predict which of them should have been detected by *ISO* in the mid-IR; this exercise was only modestly successful.

We conclude by presenting the rest-frame K-band lumi-

nosity as a function of z. We see the effect of selecting a field (i.e., the HDF-N) to be devoid of bright galaxies. We see encouraging overall consistency with predictions of evolutionary corrections for the rest-frame $L(K)$ computed from models of integrated light of galaxies by Poggianti (1997). We see the gradual change in the population of various types of galaxies, with star-forming galaxies becoming both a larger fraction of the total population and more luminous as one moves toward $z \sim 1$. The overall pattern of the $L(K)$-z relationship suggests that passive evolution at constant total stellar mass is a good approximation to the actual behavior of at least the most luminous galaxies in this large sample of galaxies in the region of the HDF-N out to $z \sim 1.5$, an issue that will be explored in depth in the next paper in this series.

The entire Keck/LRIS user community owes a huge debt to Jerry Nelson, Gerry Smith, Bev Oke, and many other people who have worked to make the Keck Telescope and LRIS a reality. We are grateful to the W.M. Keck Foundation, and particularly its late president, Howard Keck, for the vision to fund the construction of the W.M. Keck Observatory.

We thank Roger Blandford, David Hogg, and Gerry Neugebauer for helpful discussions, as well as Amy Barger and Len Cowie for access to their unpublished photometric database for the region of the HDF-N. We also thank Robert Brunner for supplying filter transmission curves and two anonymous referees for constructive criticism of the manuscript. This work was not supported by any federal agency.

APPENDIX A

UPDATES TO THE REDSHIFT CATALOG IN THE REGION OF THE HDF-N

In Tables 6A and 6B, we present redshifts obtained since 1999 November for objects in the region of the HDF-N. This is new, additional material that supplements that presented in Cohen et al. (2000). The galaxy spectral classes and redshift quality classes used here are those defined in Cohen et al. (1999a). Table 6A contains information for 53 objects in the flanking fields and is based exclusively on our LRIS (Oke et al. 1995) observations at the Keck Observatory during the winter of 2000. Emphasis in planning the observations was on galaxies with $23.0 < R < 23.5$. Table 6B contains the additional redshifts for five objects in the HDF-N itself, some of which are from other groups, as indicated in the table.

Combining this new material with the data presented in Cohen et al. (2000), the redshift completeness in the HDF-N itself to $R < 24$ is now 95%, while that in the flanking fields within the survey area of Cohen et al. is in excess of 93% to $R < 23$. The SED parameters for these new galaxies with $z < 1.5$ and reliable SEDs are given in Tables 7A and 7B.

In addition, three redshifts from the catalog of Cohen et al. (2000) are being changed. The spectral features that led to the redshift assignment given in our catalog in each case are real, but the identification assigned to them has been modified. Based on a suggestion from M. Dickinson (2000, private communication), the same suggestion subsequently being made by Fernández-Soto et al. (2001), and after looking at the relevant spectra, the redshift of H36396_1230 has been changed. What in hindsight should have been recognized as an obvious Lyα emission line was previously identified as the Mg II line at 2800 Å. The redshifts of H36494_1316 and H36560_1329 are also being modified to identify the single emission line as [O II] 3727 Å instead of Hα in order to conform to the rules stated in earlier papers in this series regarding redshifts from spectra showing only single emission lines and also based on the photometric redshift/spectroscopic redshift discrepancy discussed by Fernández-Soto et al. If these rules had been followed in all three cases, no modifications would have been necessary. The corrections are listed in Table 8. The SEDs have been calculated using the updated values.

Finally, the magnitude given for H36453_1153 in Cohen et al. (2000) is too bright. There are several faint objects close together that are clearly resolved in the *HST* image, but only one entry appears in the H00 photometric catalog. The object with the spectroscopic redshift is the U-dropout, and instead of $R = 22.53$, the value given in Cohen et al. (2000), a better estimate for this galaxy is $R \sim 23.3$.

APPENDIX B

EFFECTIVE WAVELENGTHS OF THE FILTERS

The effective wavelength of the K_s (short K) filter is taken as 2.17 μ with an absolute flux at 0 mag of $\log(\nu f_\nu) = -9.01$ W m^{-2} (M. Pahre 1998, private communication). Persson et al. (1998) also discuss the effective wavelengths of various infrared photometric systems. The effective wavelengths of the other three filters in the H00 database (U_n, G_n, and R) are given by Steidel & Hamilton (1993). The Barger et al. (1999) database consists of at least six colors, five of which are on the Johnson system, and hence their effective wavelengths can be taken from standard sources; we adopt those of Fukugita et al. (1995). The notched HK' filter is described in Barger et al. (1999; see also Wainscoat & Cowie 1992). The galaxy measurements at HK' were transformed to a standard Johnson K using the relationship $K = HK' - 0.3$ given by Barger et al. (1999).

APPENDIX C

DETAILS OF THE SED-FITTING PROCEDURES

Here we describe the details of the fitting procedures and how the flux at the transition wavelength is handled.

For the 2p SED, the power law was fit first to the side (blue or red) of rest-frame 4000 Å that had the most observed points; this depended on the redshift of the object and the number of filters for which data actually exists. A linear least-squares fitting

TABLE 6A

ADDITIONAL REDSHIFTS FOR GALAXIES IN THE FLANKING FIELDS OF THE HDF-N

R.A. (J2000)	Decl. (J2000)	R (mag)	z	Quality	Spectral Type	Source
12 36 16.67	+62 13 10.5	23.34	0.437	1	*E*	Cal
12 36 18.16	+62 12 57.6	23.54	0.473	1	*E*	Cal
12 36 21.69	+62 12 18.2	23.32	1.008	1	*E*	Cal
12 36 22.86	+62 11 18.4	23.78	0.895	5	*E*	Cal
12 36 22.85	+62 14 51.3	23.50	0.652	1	*E*	Cal
12 36 23.98	+62 11 21.6	23.53	0.842	4	*E*	Cal
12 36 25.14	+62 12 27.5	23.63	1.091	3	*A*	Cal
12 36 25.97	+62 12 37.6	23.63	0.437	1	*E I*	Cal
12 36 27.50	+62 10 26.0	23.43	0.763	3	*I*	Cal
12 36 29.75	+62 12 00.3	23.16	1.016	1	*E I*	Cal
12 36 29.82	+62 11 53.4	23.17	0.529	1	*E*	Cal
12 36 33.23	+62 10 49.9	23.34	1.006	1	*E*	Cal
12 36 36.69	+62 11 11.3	23.24	0.846	1	*E*	Cal
12 36 37.07	+62 16 15.1	23.56	0.852	1	*E*	Cal
12 36 37.72	+62 09 45.8	23.39	0.513	1	*E*	Cal
12 36 38.60	+62 12 53.3	23.41	0.960	5	*E*	Cal
12 36 39.47	+62 10 16.0	23.33	0.485	1	*E*	Cal
12 36 41.42	+62 10 51.2	23.38	0.937	1	*E*	Cal
12 36 42.34	+62 16 22.3	23.34	0.855	1	*E*	Cal
12 36 42.84	+62 14 12.1	23.43	0.586	1	*E*	Cal
12 36 43.24	+62 13 32.5	23.43	0.905	4	*E*	Cal
12 36 44.42	+62 10 52.8	23.50	0.937	1	*E*	Cal
12 36 45.24	+62 11 08.7	23.41	0.513	1	*E I*	Cal
12 36 46.56	+62 10 49.1	23.70	0.945	1	*I*	AS[a]
12 36 48.57	+62 10 48.8	23.39	0.940	5	*E*	Cal
12 36 49.75	+62 11 06.7	23.37	1.018	3	*E*	Cal
12 36 50.52	+62 15 24.0	23.80	0.321	1	*E*	Cal
12 36 52.03	+62 10 59.1	23.67	0.955	5	*E*	Cal
12 36 52.24	+62 09 57.6	23.07	0.750	1	*E*	Cal
12 36 53.36	+62 10 25.8	23.20	0.973	4	*E*	Cal
12 36 56.03	+62 10 20.7	23.64	0.938	1	*E*	Cal
12 36 56.84	+62 10 02.0	23.51	0.000	1	*M*	Cal
12 36 57.07	+62 15 11.2	23.50	0.849	1	*E I*	Cal
12 36 57.30	+62 10 26.1	23.29	0.847	5	*E*	Cal
12 36 57.70	+62 10 40.9	23.24	1.416	3	*A*	Cal
12 36 58.52	+62 15 53.3	23.55	0.457	1	*E*	Cal
12 36 59.83	+62 09 47.9	23.04	0.679	1	*E*	Cal
12 37 00.16	+62 16 15.1	22.83	0.914	1	*E*	Cal
12 37 00.42	+62 10 01.6	23.26	0.791	5	*E*	Cal
12 37 00.77	+62 11 33.7	23.27	0.305	1	*E*	Cal
12 37 00.90	+62 10 28.4	22.27	0.563	1	*E I*	Cal
12 37 01.11	+62 14 26.0	23.41	0.901	4	*E*	Cal
12 37 02.24	+62 10 33.0	23.46	0.276	1	*E*	Cal
12 37 02.53	+62 11 05.3	23.43	1.014	1	*E*	Cal
12 37 04.25	+62 09 59.7	22.59	0.322	1	*E*	Cal
12 37 04.27	+62 10 29.9	23.23	0.411	1	*E*	Cal
12 37 06.04	+62 13 40.4	23.25	0.672	5	*E*	Cal
12 37 06.33	+62 10 57.4	23.66	0.906	1	*E*	Cal
12 37 06.83	+62 10 06.6	22.89	0.938	4	*E*	Cal
12 37 09.64	+62 11 19.4	23.76	1.176	1	*E*	Cal
12 37 10.54	+62 11 16.3	23.60	0.841	5	*E*	Cal
12 37 11.14	+62 12 57.0	23.20	0.484	1	*E*	Cal
12 37 12.15	+62 11 44.2	23.10	0.909	4	*E*	Cal

[a] This redshift is from Adelberger & Steidel 2000.

routine from Press et al. (1986) was used. Once one index was determined, the second spectral index is calculated, assuming forced agreement in the value of L_ν at 4000 Å.

For the sBB SED model, the fitting is accomplished with routines from Press et al. (1986). The fitting rules are as follows: If there are four or more filter bands observed on the red side and three or more on the blue side, then the regimes $\lambda < \lambda_m$ and $\lambda > \lambda_m$ are fit independently. If there are fewer than four on the red side, then the blue side is fit first. A point is then added to the red side at λ_m with the luminosity there being that calculated from the blue fit. Then the red fit is done. If there are fewer than three on the blue side, then the red side fit is done first, and a point is added to the blue side at λ_m with the value predicted from the sBB fit.

TABLE 6B

ADDITIONAL REDSHIFTS FOR GALAXIES IN THE HDF-N

R.A. (J2000)	Decl. (J2000)	R (mag)	z	Quality	Spectral Type	Source
12 36 37.77	+62 12 35.1	23.87	0.485	1	*E*	Cal
12 36 45.30	+62 11 42.9	24.00	0.558	1	*E*	St0, Cal
12 36 47.17	+62 13 41.7	23.93	1.313	1	*EA*	Daw[b]
12 36 43.84	+62 12 41.5	25.21	4.540	11	*E*	Stern[c]
12 36 44.66	+62 11 50.2	26.50	4.580	11	*E*	Stern[c]

[b] From Dawson et al. 2001.
[c] Published in Stern & Spinrad 1999.

TABLE 7A

SED PARAMETERS FOR ADDITIONAL GALAXIES IN THE FLANKING FIELDS OF THE HDF-N

R.A. (J2000)	Decl. (J2000)	log $L(B)$[a] (W)	α_{UV} (2p)	α_{IR} (2p)	α_{UV} (sBB)	log $L(\lambda_m$, blue) (W)	T (sBB)	log $L(\lambda_m$, red) (W)
12 36 16.67	+62 13 10.5	35.68	2.27	−0.34	1.09	35.54	9162	35.60
12 36 18.16	+62 12 57.6	35.67	1.82	0.93	0.50	35.46	5281	35.51
12 36 21.69	+62 12 18.2	36.60	1.61	0.96	1.73	36.61	6873	36.61
12 36 22.86	+62 11 18.4	36.24	1.76	1.17	1.71	36.22	6255	36.29
12 36 22.85	+62 14 51.3	36.01	2.12	0.77	1.60	35.91	6143	35.97
12 36 23.98	+62 11 21.6	36.18	0.73	0.92	0.57	36.15	6708	36.25
12 36 25.14	+62 12 27.5	36.50	2.18	−0.13	2.41	36.59	13001	36.59
12 36 25.97	+62 12 37.6	35.37	1.39	0.77	1.02	35.29	6372	35.43
12 36 27.50	+62 10 26.0	36.19	4.16	1.53	4.16	36.18	5732	36.26
12 36 29.75	+62 12 00.3	36.53	0.08	0.89	0.18	36.56	6927	36.56
12 36 29.82	+62 11 53.4	35.74	0.79	0.66	0.38	35.67	6915	35.82
12 36 33.23	+62 10 49.9	36.58	1.30	1.19	1.66	36.64	6421	36.64
12 36 36.69	+62 11 11.3	36.31	0.92	0.61	0.87	36.32	8018	36.44
12 36 37.07	+62 16 15.1	36.22	1.33	1.22	1.33	36.21	6107	36.31
12 36 37.72	+62 09 45.8	35.85	2.40	−0.40	0.40	35.58	8350	35.73
12 36 38.60	+62 12 53.3	36.34	1.42	−0.26	1.17	36.37	12158	36.37
12 36 39.47	+62 10 16.0	35.75	2.30	−0.02	0.66	35.53	6753	35.64
12 36 41.42	+62 10 51.2	36.47	2.32	1.60	2.32	36.45	5699	36.64
12 36 42.34	+62 16 22.3	36.43	3.38	0.82	3.38	36.45	7613	36.52
12 36 43.24	+62 13 32.5	36.29	0.66	1.29	0.58	36.27	6278	36.40
12 36 44.42	+62 10 52.8	36.31	0.86	0.60	0.84	36.32	8136	36.40
12 36 45.24	+62 11 08.7	35.56	0.03	−0.22	−0.17	35.61	10293	35.76
12 36 46.56	+62 10 49.1	36.48	2.83	2.59	2.82	36.38	4616	36.59
12 36 49.75	+62 11 06.7	36.56	0.56	1.10	0.49	36.55	5826	36.55
12 36 52.03	+62 10 59.1	36.33	1.09	1.24	1.69	36.46	6679	36.46
12 36 52.24	+62 09 57.6	36.31	2.46	1.47	2.48	36.31	5119	36.31
12 36 53.36	+62 10 25.8	36.54	0.94	0.84	1.19	36.60	7075	36.60
12 36 56.03	+62 10 20.7	36.30	1.13	1.27	1.13	36.28	6664	36.47
12 36 57.07	+62 15 11.2	36.24	1.10	1.16	1.00	36.22	6184	36.35
12 36 57.30	+62 10 26.1	36.34	1.84	1.92	1.84	36.30	5459	36.52
12 36 57.70	+62 10 40.9	37.25	3.14	0.75	3.65	37.44	9231	37.44
12 36 58.52	+62 15 53.3	35.67	3.75	−0.34	2.10	35.49	8619	35.57
12 37 00.16	+62 16 15.1	36.61	1.06	1.10	1.04	36.60	6556	36.60
12 37 00.42	+62 10 01.6	36.24	0.74	1.04	0.68	36.21	6253	36.28
12 37 00.90	+62 10 28.4	36.31	2.80	0.98	1.50	36.08	5429	36.22
12 37 01.11	+62 14 26.0	36.32	0.80	0.98	0.70	36.31	6565	36.41
12 37 02.24	+62 10 33.0	35.23	2.51	0.06	1.33	35.13	7636	35.15
12 37 02.53	+62 11 05.3	36.37	0.13	−0.09	0.41	36.48	12724	36.48
12 37 04.25	+62 09 59.7	35.69	2.84	−0.30	1.93	35.63	10928	35.68
12 37 04.27	+62 10 29.9	35.67	2.05	−0.02	1.49	35.64	8218	35.62
12 37 06.04	+62 13 40.4	36.21	2.19	−0.25	1.96	36.20	9040	36.15
12 37 06.33	+62 10 57.4	36.27	0.96	0.66	0.93	36.29	8017	36.38
12 37 06.83	+62 10 06.6	36.56	0.82	1.12	0.82	36.55	6209	36.67
12 37 09.64	+62 11 19.4	36.66	1.23	1.41	1.22	36.64	5581	36.64
12 37 10.54	+62 11 16.3	36.12	0.62	0.37	0.62	36.15	9395	36.30
12 37 11.14	+62 12 57.0	35.61	0.37	1.15	0.37	35.60	6021	35.70
12 37 12.15	+62 11 44.2	36.49	1.74	0.90	1.61	36.49	6268	36.50

[a] $M_B = -21.0$ (rest frame) $\equiv$ log $[L(B)$ (W)$] = 36.9$.

TABLE 7B

SED Parameters for Additional Galaxies in the HDF-N

R.A. (J2000)	Decl. (J2000)	log $L(B)$[a] (W)	α_{UV} (2p)	α_{IR} (2p)	α_{UV} (sBB)	log $L(\lambda_m$, blue) (W)	T (sBB)	log $L(\lambda_m$, red) (W)
12 36 45.30	+62 11 42.9	35.67	1.31	0.59	−0.03	35.43	6612	35.57
12 36 47.17	+62 13 41.7	36.69	0.80	1.14	0.68	36.64	7056	36.73

[a] $M_B = -21.0$ (rest frame) $\equiv$ log [$L(B)$ (W)] = 36.9.

TABLE 8

Corrections to Redshifts for Galaxies in the HDF-N

R.A. (J2000)	Decl. (J2000)	R (mag)	Adopted z	Quality	Spectral Type
12 36 39.60	+62 12 30.2	24.40	3.479	11	*E*
12 36 49.43	+62 13 16.5	23.63	1.238	3	*E*
12 36 56.10	+62 13 29.6	23.80	1.238	4	*E*

REFERENCES

Aaronson, M. 1978, ApJ, 221, L103
Adelberger, K., & Steidel, C. C. 2000, ApJ, 544, 218
Aussel, H., Cesarsky, C. J., Elbaz, D., & Starck, J. L. 1999, A&A, 342, 313
Barger, A. J., Cowie, L. L., & Richards, E. A. 2000, AJ, 119, 2092
Barger, A. J., Cowie, L. L., Trentham, N., Fulton, E., Hu, E. M., Songaila, A., & Hall, D. 1999, AJ, 117, 102
Bertin, E., & Arnouts, S. 1996, A&AS, 117, 393
Blain, A. W., Kneib, J. P., Ivison, R. J., & Smail, I. 1999, ApJ, 512, L87
Blanton, M. R., et al. 2001, AJ, 121, 2358
Boselli, A., Gavazzi, G., Donas, J., & Scodeggio, M. 2001, AJ, 121, 753
Brown, W. R., Kenyon, S. J., Geller, M. J., & Fabricant, D. G. 2000, ApJ, 540, L83
Brunner, R. J., Szalay, A. S., & Connolly, A. J. 2000, ApJ, 541, 527
Budavári, T., Szalay, A. S., Connolly, A. J., Csabai, I., & Dickinson, M. 2000, AJ, 120, 1588
Calzetti, D. 1997, AJ, 113, 162
Calzetti, D., Kinney, A. L., & Storchi-Bergmann, T. 1994, ApJ, 429, 582
Carlberg, R. G., et al. 2000, ApJ, 532, L1
Cohen, J. G., Blandford, R., Hogg, D. W., Pahre, M. A., & Shopbell, P. L. 1999a, ApJ, 512, 30
Cohen, J. G., Hogg, D. W., Blandford, R., Cowie, L. L., Hu, E., Songaila, A., Shopbell, P., & Richberg, K. 2000, ApJ, 538, 29
Cohen, J. G., Hogg, D. W., Pahre, M. A., Blandford, R., Shopbell, P. L., & Richberg, K. 1999b, ApJS, 120, 171
Cole, S. et al. 2001, MNRAS, in press
Coleman, G. D., Wu. C. C., & Weedman, D. W. 1980, ApJS, 43, 393
Connolly, A. J., Szalay, A. S., Dickinson, M., SubbaRao, M. U., & Brunner, R. J. 1997, ApJ, 486, L11
Côté, P., Oke, J. B., & Cohen, J. G. 1999, AJ, 118, 1645
Cowie, L. L., Songaila, A., Hu, E. M., & Cohen, J. G. 1996, AJ, 112, 839
Dawson, S. Stern, D., Bunker, A. Spinrad, H., & Dey, A. 2001, in preparation
Dey, A., Graham, J. R., Ivison, R. J., Smail, I., Wright, G. S., & Liu, M. C. 1999, ApJ, 519, 610
Dickinson, M. E. 2000, in Building Galaxies: From the Primordial Universe to the Present, ed. F. Hammer, T. X. Thuan, V. Cayette, B. Guiderdoni, & J. Trân Thanh Vân (Gif-sur-Yvette: Ed. Frontières), 257
Ellis, R. S., Colless, M., Broadhurst, T., Heyl, J., & Glazebrook, K. 1996, MNRAS, 280, 235
Elmegreen, B. G. 2000, ApJ, 539, 342
Fernández-Soto, A., Lanzetta, K. M., Chen, H. W., Pascarelle, S., & Yahata, N. 2001, ApJS, in press
Fernández-Soto, A., Lanzetta, K. M., & Yahil, A. 1999, ApJ, 513, 34
Folkes, S., et al. 1999, MNRAS, 308, 459
Frogel, J. A., Persson, S. E., Aaronson, M., & Matthews, K. 1978, ApJ, 220, 75
Fukugita, J., Shimasaku, K., & Ichikawa, T. 1995, PASP, 107, 945
Gardner, J. P., Sharples, R. M., Frenk, C. S., & Carrasco, B. E. 1997, ApJ, 480, L99
Hammer, F., et al. 1997, ApJ, 481, 49
Hogg, D. W. 2001, AJ, 121, 1207
Hogg, D. W., Cohen J. G., & Blandford R. 2000, ApJ, 545, 32
Hogg, D. W., et al. 1998a, AJ, 115, 1418
Hogg, D. W., Cohen, J. G., Blandford, R., & Pahre, M. A. 1998b, ApJ, 504, 622
Hogg, D. W., Neugebauer, G., Cohen, J. G., Dickinson, M., Djorgovski, S. G., Matthews, K., & Soifer, B. T. 2000a, AJ, 119, 1519
Hogg D. W., et al. 2000b, ApJS, 127, 1 (H00)
Hornschemeier, A. E., et al. 2000, ApJ, 541, 49
Hughes, D., et al. 1998, Nature, 394, 241
Lilly, S. J., Eales, S. A., Gear, W. K. P., Hammer, F., Le Fèvre, O., Crampton, D., Bond, J. R., & Dunne, L. 1999, ApJ, 518, 641
Lin, H., Kirshner, R. P., Shectman, S. A., Landy, S. D., Oemler, A., & Shechter, P. L. 1996, ApJ, 464, 60
Loveday, J. 2000, MNRAS, 312, 557
Meurer, G. R., Heckman, T., & Calzetti, D. 1999, ApJ, 521, 64
Moriondo, G., Cimatti, A., & Daddi, E. 2000, A&A, 364, 26
Oke, J. B., et al. 1995, PASP, 107, 375
Persson, S. E., Murphy, D. C., Krzeminski, W., Roth, M., & Rieke, M. J. 1998, AJ, 116, 2475
Poggianti, B. M. 1997, A&AS, 122, 399
Press, W. H., Flannery, B. P., Teukolsky, S. A., & Vetterling, W. T. 1986, Numerical Recipes in Fortran (Cambridge: Cambridge Univ. Press)
Richards, E. A. 2000, ApJ, 533, 611
Richards, E. A., Fomalont, E. B., Kellerman, K. I., Windhorst, R. A., & Partridge, R. B. 1998, AJ, 116, 1039
Richards, E. A., Fomalont, E. B., Kellerman, K. I., Windhorst, R. A., Partridge, R. B., Cowie, L. L., & Barger, A. J. 1999, ApJ, 526, L73
Sanders, D. B., & Mirabel, F. 1996, ARA&A, 34, 749
Scodeggio, M., & Silva, D. 2000, A&A, 359, 953
Schlegel, D. J., Finkbeiner, D. P., & Davis, M. 1998, ApJ, 500, 525
Smail, I., Ivison, R. J., Kneib, J. P., Cowie, L. L., Blain, A. W., Barger, A. J., Owen, F. N. & Morrison, G. 1999, MNRAS, 308, 1061
Steidel, C. C., Adleberger, K. L., Giavalesco, M., Dickinson, M., & Pettini, M. 1999, ApJ, 519, 1
Steidel, C. C., & Hamilton, D. 1993, AJ, 105, 2017
Stern, D., & Spinrad, H. 1999, PASP, 111, 1475
Stiavelli, M., & Treu, T. 2000, in ASP Conf. Ser., Galaxy Disks and Disk Galaxies, ed. J. G. Funes, S. J. & E. M. Corsini (San Francisco: ASP), in press
Sullivan, M., Treyer, M. A., Ellis, R. S., Bridges, T. J., Milliard, B., & Donas, J. 2000, MNRAS, 312, 442
van den Bergh, S., Cohen, J. G., Hogg, D. W., & Blandford, R. 2000, AJ, 120, 2190
Wainscoat, R. J., & Cowie, L. L. 1992, AJ, 103, 332
Williams, R. E., et al. 1996, AJ, 112, 1335
Worthey, G. W. 1994, ApJS, 95, 107
Zaritsky, D., Kennicutt, R. C., Jr., & Huchra, J. P. 1994, ApJ, 420, 87